



Universität für Bodenkultur Wien



Department für Nanobiotechnologie (DNBT)

Institut für Synthetische Bioarchitekturen

Vorstand: Univ.Prof. Dr.rer.nat. Eva-Kathrin Ehmoser

Betreuerin: Univ.Prof. Dr.rer.nat. Eva-Kathrin Ehmoser

High- k passivated electrodes:

**On the electrodynamic behavior of cells under the
influence of capacitively coupled electric fields**

Dissertation

zur Erlangung des Doktorgrades
an der Universität für Bodenkultur Wien

Durchgeführt am Austrian Institute of Technology

Health & Environment Department, Molecular Diagnostics

Eingereicht von
Mag.rer.nat. Terje Wimberger

Wien, November 2020

©Terje Wimberger

All rights reserved

2020

Affidavit

I give my solemn word that I have compiled this work solely and without external help, have not utilized any sources outside those permitted and that the sources used have been given verbatim or quoted textually in the places indicated.

This work has not been submitted in the same or similar form to any other examiners as a form of examination.

Vienna, November 2020

Terje Wimberger

Acknowledgement

First and foremost, my thanks go to Prof. Ehmoser and the BOKU Institute of Synthetic Bioarchitectures for their supervision, training and support over the entirety of the project. The same goes for all my colleagues at the Competence Unit Molecular Diagnostics of the Austrian Institute of Technology, with special academic shoutouts to Ciril Reiner-Rozman, Johannes Peham and Winfried Neuhaus for their exceptional insights in conjunction with my research topic. Special thanks extend to Lisa Milchram, Julie Krainer, Christopher Herz, Michaela Hendling, Jennifer Beyerknecht, Noa Wolff, Christina Bliem, Peter Hetegger, Martin Jung, Grace Lin and all others who were of equal assistance during both the brightest and darkest times of my thesis.

My greatest appreciation goes to all interns under my proud supervision. Thanks to Jan Pilsinger, Vivien Juhász, Dalma Cséczy, Nathalie Tichy, Laura Wellenzohn and Julia Dolezel who equally catalyzed advancements to the project and my personal growth as a teacher and supervisor. A special thank you extends to Verena Köhler for her efforts towards producing a significant part of the excellent data that went into the second featured manuscript.

A big hug to all my friends who supported this thesis with academic or emotional support, including Philipp Heher, Bernhard Stich, Paul Prichenfried, Max Haider and Roland Prielhofer.

I am grateful and proud of my captain Klemens Wassermann, who for the past five years chose to be more of a friend and a leader than my boss and mentor. This allowed me to assume what remained of the latter roles for myself, immensely facilitating my personal and academic fulfillment.

Last and certainly not least, I thank my family for their endurance and support through many years of joy and hardships. Sylvia and Liv – I love you!

Considerable complexity is expected (Eisenberg 2016)

Kurzfassung

Elektroporation bezeichnet die Manipulation lebender Zellen mittels elektrischer Felder. StudentInnen der Biologie sind durch mikrobiologische Einführungskurse mit dem Vorgang der elektrischen Transformation von Bakterien vertraut. Hat man das Einbringen von DNA in ein Bakterium zum Ziel, empfiehlt sich folgende Vorgehensweise; Die Bakteriensuspension samt fremd-DNA in einer Küvette mit Metallelektroden vermischen, den Knopf drücken und anschließend die schäumende Flüssigkeit mit der genetisch veränderten Bakterienkultur weiterzüchten. Doch wie können wir uns diesen Vorgang erklären? Werden lebende Zellen einer ausreichenden elektrischen Feldstärke ausgesetzt, führt das zur Porenbildung in der Äußeren Zellmembran. Dieser Zusammenbruch der selektiven Barrierefunktion ermöglicht das Eindringen von geladenen Teilchen aus der umliegenden Lösung. Die Entstehung dieser "Elektroporen" kann, entsprechend der gewählten Intensität der Behandlung, zur elektrischen Lyse, Zellfusion oder eben zum Einschleusen von genetischem Material verwendet werden. Doch wieso wird dieses vielfältige und einfache Gerät danach wieder im Schrank eures Mikrobiologie-Tutors weggeschlossen? Erinnert ihr euch an die "schäumende" Flüssigkeit aus dem Einführungskurs? Die Antwort ist dieselbe – Elektrochemie. Während der Elektroporation wird in der Lösung elektrische Energie in thermische und chemische Energie umgewandelt. Diese Formen der Energieumwandlung sind deshalb problematisch, weil deren Einflüsse auf die enthaltene Zellpopulation nicht kontrollierbar sind. Nehmen wir an, du möchtest mittels elektrischer Felder ein Plasmid in eine tierische Zellpopulation einschleusen. Ob dieses Vorhaben an einer einzelnen Zelle erfolgreich ist, hängt neben der gewählten Feldeinstellung beispielsweise von der lokalen Temperatur, dem pH-Wert und der Nähe zur Oberflächenspannung einer Luftblase ab. Spätestens wenn wir erfahren, dass all diese Einflüsse zeitabhängig variieren, wird die Komplexität des Vorhabens offensichtlich. Die Anzahl an getöteten und erfolgreich manipulierten Zellen wird bei wiederholter Anwendung stark variieren. Das macht die praktische Umsetzung zu einem frustrierenden Erlebnis und ist der Grund dafür, dass die Methode in weiteren Praktika und der späteren wissenschaftlichen Anwendung überwiegend vermieden wird. Die vorliegende Arbeit befasst sich mit einer technologischen Innovation, welche die Komplexität der Methode um jene Faktoren reduziert, die auf elektrochemischen Vorgängen basieren; Elektroden werden mit einem dielektrischen Material beschichtet und dadurch elektrisch passiviert. In Folge kommt der spezifische Einfluss elektrischer Felder zur Geltung und manifestiert sich in einer hohen Reproduzierbarkeit der Ergebnisse.

Das Konzept wurde in Form von zwei mikrofluidischen Prototypen umgesetzt; einer Pipettenspitze zur stationären Anwendung und einer Durchflusskonfiguration für erhöhten Probendurchsatz. Die jeweiligen Publikationen umfassen das Ausmaß der verbleibenden, elektrochemischen Übergänge und demonstrieren die Vorteile der beiden Konfigurationen für verschiedene Anwendungen. Durch die hohe Reproduzierbarkeit der Ergebnisse wird es möglich, den Zusammenhang diverser Feldparameter mit dem Anteil der betroffenen Zellfraktion zu vergleichen. Im ersten Manuskript wird die Lyse von HEK-293 Zellen in Abhängigkeit von Spannung, Pulszahl, Frequenz und Pufferleitfähigkeit präzisiert. Das Ergebnis ist die erste umfassende Beschreibung von Elektroporation mittels passivierter Elektroden.

Die Zweite Publikation befasst sich mit dem Einfluss biologischer Variabilität in einem Durchflusssystem. Verschiedene Zellpopulationen werden identischen elektrischen Feldeinflüssen ausgesetzt und zeigen hier überraschend unterschiedliches Lyseverhalten. Diese Unterschiede werden zur selektiven Lyse von Erythrozyten, Leukozyten, Jurkat T-Lymphozyten und MCF-7 Zellen genutzt. Die Reihenfolge der Feldanfälligkeit dieser Zelltypen unterscheidet sich fundamental von Berichten zur selektiven Lyse in Systemen ohne Passivierung.

Abstract

Most students of biology have come across electroporation at least once when performing genetic manipulation of bacteria in a basic lab course; Mix the bacterial suspension with foreign DNA in a cuvette with flanking electrodes, press the magic button and extract genetically modified bacteria from a foamy solution. Incredible. How does this work and why? Electroporation refers to the manipulation of living cells by electric fields. The outer membrane of these cells will undergo dielectric breakdown when exposed to an externally applied electric field of sufficient magnitude. This manifests in the creation of pores through which otherwise confined molecules can enter or leave the cell - hence the term electroporation. The possible outcomes of pore formation are highly diverse, ranging from cell lysis and cell fusion to cargo delivery or -extraction, including said transfer of genetic material. But why is this versatile method confined to the cupboard of your microbiology tutor? Remember the 'foamy' bit about the transformation experiment? Same answer: Electrochemistry. When we press the magic button, we are inevitably transferring electrical energy to the solution where it is converted to thermal and chemical energy. The latter consists of pH change and bubble formation causing the visual feedback. The problem with changes in temperature and these types of chemical processes is that their biological impact cannot be controlled, meaning they introduce a significant chaos-factor into the equation. Say you want to perform an experiment toward electric field mediated gene delivery in mammalian cells. The outcome of a single delivery event will at least depend on local field strength, temperature, pH and the vicinity to a gas bubble - all of which are time-varying parameters. Sound complicated? Precisely is not a suitable term in this context. The amount of dead and successfully manipulated cells won't square up between multiple repetitions, resulting in a highly frustrating user experience. The technological advancement presented in this thesis is a removal of the chaos factor by what we term high-k dielectric electrode passivation. This results in capacitive coupling, essentially describing an electric field application where the transformation of electrical energy into its detrimental forms, like thermal and chemical energy, is significantly reduced.

The concept is implemented in two microfluidic prototype designs for stationary and continuous sample treatment. Each presented manuscript is based on one of these designs, quantifies the extent to which electrochemistry is reduced and demonstrates the resulting advantages for the presented applications. As previously suggested, the most distinguishing difference is the increased reproducibility of both mammalian cell lysis- and permeabilization events. This enables us to match defined changes in a physical parameter to its biological impact. In the first presented manuscript, these dependencies were investigated for HEK-293 epithelial cells as a biological model, defining how variables like field strength, conductivity, frequency and pulse number influence the percentage of affected cells. This represents the first in-depth experimental characterization of capacitively coupled electroporation effects to date.

The second manuscript proceeds to introduce biological variability, examining how the lysis susceptibility of different mammalian cell populations varies in response to the same physical parameters. Making use of the precise outcomes that are the result of electrode passivation, differences in lysis dynamics are exploited toward the differential lysis of erythrocytes, leukocytes, Jurkat T Lymphocytes and MCF-7 cells. The order of lysis observed for these populations is entirely different from previous reports on selective electroporation via ohmic coupling.

Table of contents

Acknowledgement	V
Kurzfassung	VII
Abstract	IX
1. Introduction	1
1.1 Electric fields and common variables in electroporation.....	1
1.2 Membrane electropermeabilization is dose dependent.....	2
1.2 Lipid membranes.....	3
1.3 Mechanics of electroporation	4
1.4 Applications of electroporation.....	5
1.5 Current challenges.....	6
1.6 Current remedies	8
1.7 Capacitive coupling.....	9
2. Publications	11
2.1 Controllable cell manipulation in a microfluidic pipette-tip design using capacitive coupling of electric fields	11
2.2 Capacitive coupling increases the accuracy of cell-specific tumour disruption by electric fields	23
3. Discussion	33
3.1 Electrodynamic implications	33
3.2 Biological implications.....	34
4. Conclusion and outlook	37
5. References	39
6. Curriculum Vitae	45

1. Introduction

The vast amounts of accumulated knowledge in individual scientific fields make it increasingly difficult for scientists of neighboring disciplines to understand the significance of novel findings. This is increasingly pronounced in interdisciplinary fields, where basic knowledge of converging disciplines is frequently acquired at great personal expense. The primary aim of this introduction to electroporation and the technological content of this project is meant to equip the readers mind with the framework required to understand the publications submitted over the course of this thesis. A special emphasis is placed on simple descriptions of the systems electrodynamic behavior that should assist academics in biology to realize how such mechanics result in the presented applications for cell manipulation.

1.1 Electric fields and common variables in electroporation

When electric fields are mentioned in the context of cell manipulation, they are almost exclusively generated via the application of electric current to terminal electrodes. The resulting electric potential difference between these electrodes is annotated as the applied electric potential (U) in Volt [V] which is proportional to the electric field magnitude $E = U/d$, further defined by the distance (d) between the electrodes. Field uniformity is determined by electrode geometry and considered homogeneous in a parallel configuration, historically the most common spatial arrangement. Since experiments in this thesis are also based on parallel electrode designs, a higher voltage simply implies that all cells are subjected to a relatively stronger electric field for the exposure duration. Typically, high voltage pulses of square waves (constant U over a defined duration, t) or exponential decay functions (decreasing U over a defined duration) are applied. Common conditions for electric field treatment are distinguished by electric field magnitude (E), duration (t), number of repetitions (N) and frequency (f) or, inversely, their period ($P = 1/f$). [1] Each parameter can be controlled independently and is highly consequential to the biological outcome of electric field exposure.

Electroporation is dose dependent, meaning that the observable biological effect increases with Voltage, duration and exposure time (Fig. 1) but not frequency as it does not alter the dose but only the rate of application. Frequency dependent phenomena have more complex implications that will be discussed in context. Another characteristic feature of electric field application in biology is the direct contact between electrodes and the liquid suspension that is necessary for the survival of subject cells or tissues. The most cited variable in this context is the resistance of the liquid suspension, usually expressed as the inversed property; conductivity σ [S/m]. While sample viscosity appears to have negligible electrodynamic impact, the outcome of electrical treatment conditions is highly dependent on the local temperature T [°K]. [2]

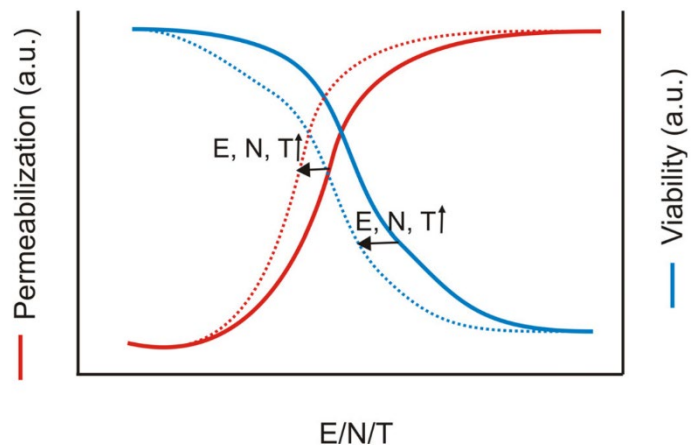


Figure 1 Schematic graph of cell membrane permeabilization and cell viability. Both strongly depend on electric field strength (E), the number of pulses (N), and the pulse duration (T). The higher values these parameters have, the more cells are permeabilized, but the less cells survive. From Rosazza *et.al.*, *Current Gene Therapy*, 2016 [1]

1.2 Membrane electroporation is dose dependent

When hen biological membranes are exposed to externally imposed electric fields, the lipid bilayer becomes permeable to otherwise impermeable molecules. This means an alteration of cellular homeostasis occurs to an extent that is proportional to the supplied energy. It follows that an excess of electric field exposure will lead to cell death. Early exploitations of this effect include its use toward microbial inactivation in the food industry by Heinz Doevenspeck in the 1960ies. [2,3] Subsequent investigations by Sale and Hamilton showed that cell death by electric fields is a function of voltage level and exposure time. They confirmed that cell lysis was indeed a consequence of electric field application rather than electrolytic side effects [4] and proceeded to demonstrate that the electric field is responsible for membrane breakdown.[5] These works are the basis of the hypothesis that Maxwell's calculations on the conduction through a suspension of spheres are applicable to cell suspensions. Viewing the cell membrane as a thin, spherical

dielectric that separate two media of different conductivity, implies that an external electric field will induce a change in potential difference across the dielectric lipid bilayer. Sale and Hamilton proposed that lipid membranes lose their intrinsic barrier function when their transmembrane potential exceeds 1 V, noting that the precise value is species dependent.[6] These claims were later substantiated by Hulsheger and colleagues who proposed that the induced membrane potential depends on cell radius, formulating that $V_m = 1.5 a E_c$. [7] The potential difference across the membrane (V_m) is approximated by multiplying a shape factor of 1.5 (when solved for a spherical particle) with the cell radius a and the external electric field E_c , implying that larger cells will have a higher induced membrane voltage at the same field strength than smaller cells. This formula is still used to provide a decent approximation of the induced membrane voltage as a result of electric field exposure. It was expanded upon by Neumann in 1989, who accounted for the spatial differences in induced transmembrane potential that are a consequence of orientation, as hypothesized by Maxwell [8]:

$$\text{TMP} = 1.5 a E_c \cos \Phi \quad (1)$$

This modified formula effectively introduces the restriction that the previous approximation is only valid for a portion of the membrane that is perpendicular electric field lines. For a spherical cell between parallel electrodes, this means that areas of the membrane facing the electrodes will be most affected by the electric field (Fig. 3). Formula (1) is referred to as the Schwann equation and is only valid in this form for a spherical particle where the resistivity of the membrane is much higher than the surrounding media, as applies to a biological cell. Empirical findings demonstrate that increasing the field strength above a minimum electroporation threshold increases the permeabilized area while

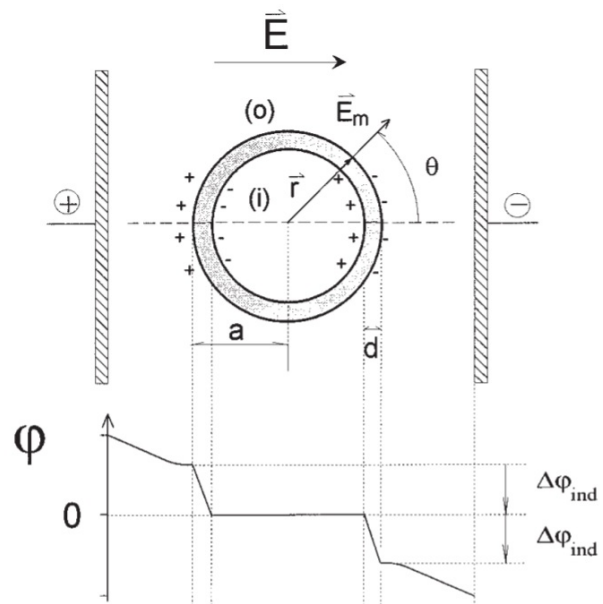
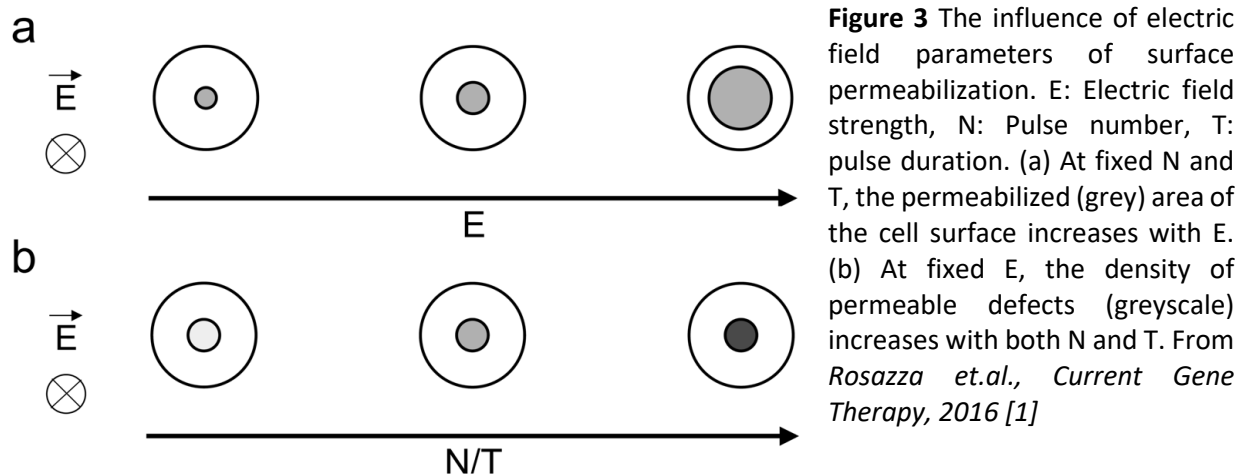


Figure 2 Electrical membrane polarization and cross membrane potential of a cell with radius a and membrane thickness d . The electrical potential profile ϕ is shown, where $\Delta\phi_{ind}$ the is the drop in the induced membrane potential in the direction of E applied external electric field. From Neumann, *Electroporation and Electrofusion in Cell Biology*, 1989 [8]



increasing field duration correlates with pore density and size (Fig. 3). Note that formula (1) has a second term that has been removed in this context for simplicity. Briefly, it includes dependencies to field frequency and membrane charging time which in turn depends on all conductivities of the system as well as membrane permittivity and thickness. This part of the formula was omitted because the frequency term is considered dispensable below 10 kHz while membrane charging time is negligible when the pulse length is larger than 1 μ s, corresponding to frequencies near the MHz-range.[9] Their significance is pronounced in nanosecond electroporation, characterized by entirely different mechanics such as organelle-specific permeabilization.[10]

1.2 Lipid membranes

Predictions on the interplay between electric fields and the outer cell membrane assume a lipid bilayer structure. The simplest and best studied are historically termed black lipid membranes (BLM) where each phospholipid consists of two hydrophilic hydrocarbon chains linked to a hydrophilic triglycine 'head'. In aqueous media, head groups will associate with each other to form planar structures with a thickness of about 5nm featuring a hydrophilic core and hydrophobic edges. From an electrical point of view, such a bilayer displays both high resistance in the Giga-ohm range and a large capacitance (1-2 μ F/cm²). [11,12] Two further properties are of particular relevance to electroporation; First, the fluid-like properties of the bilayer core and second, the complex dependence on coulombic and dipolar forces that govern interactions between the strongly interacting tails and the surrounding aqueous medium.[13] As a semi-permeable barrier, small molecules such as water may diffuse freely through the bilayer whereas the passage rate of other molecules depends primarily on their ability to enter the hydrophilic center of the membrane. This rate limiting step is considered critical to all mechanistic models on electro-pore formation in lipid bilayers.

Simulations of lipid bilayer models typically lack most membrane characteristics that functionalize live plasma membranes, such as protein components. However, it appears that the dielectric properties that impact electroporation remain reasonably constant between different cell types, with capacitance per unit area ranging between 5-10 mF m⁻² and dielectric constants between 2 - 2.2.[14] This suggests that the influence of protein inserts on the specific field magnitude required for electroporation is insignificant compared to other, more prominent factors.[11] One of these is membrane fluidity. It increases with temperature, which was previously mentioned to have a large impact on electroporation thresholds.[3] This influence extends to other mechanics that will be discussed in context, such as pore resealing dynamics. Note that the lipid composition of plasma membranes can determine membrane fluidity at constant temperature and differ significantly between species, tissues and even cell populations of the same type.[15,16]

1.3 Mechanics of electroporation

The prevailing mechanistic theory on electro-permeabilization that is in best agreement with experimental reports, proposes the creation of transient hydrophilic pores in the plasma membrane of cells.[8,17,18] The cycle of pore formation and re-sealing is characterized by three phases; (1) pore formation, (2) dose-dependent alteration of pore size and (3) pore re-sealing. The process of pore formation is initiated by ion flow to the surface of an intact membrane. This leads to charge buildup along the membrane capacitor and subsequent polarization.[19] From an electrical perspective, membrane breakdown is initiated when external polarization exceeds membrane capacitance for a sufficient amount of time. While necessarily correct, viewing the process from the point of particle dynamics gives more specific insights into the initiation of pore formation. Charged particles along the hydrophilic interface require a certain energy to reach the hydrophobic core of the bilayer. As the membrane becomes polarized, greater dielectric forces act on adjacent particles and the passage of polar or charged molecules across the hydrophobic barrier is incrementally increased as a function of probability (Fig. 4B). Such an increase of particle mobility across the bilayer leads to the creation of hydrophilic pores that do not alter the principal structure of the bilayer (Fig. 4C). A critical threshold of local charge transfer will yield a critical hydrophobic pore radius r_{crit} . At this point, the rearrangement of lipid head groups is energetically favored to create a hydrophilic pore (Fig. 4D).[20] These are characterized by rearrangement of hydrophilic head groups toward the inside of the pore, forming a channel that allows for the passage of larger molecules and ions. The resulting charge flux through the pore in turn leads to relaxation of the field-induced membrane polarization. Since lipid bilayers behave as two-dimensional liquids, the local membrane will return to its initial conformation unless input energy is greater than the relaxation caused by the charge flow (Fig. 5). These processes characterize

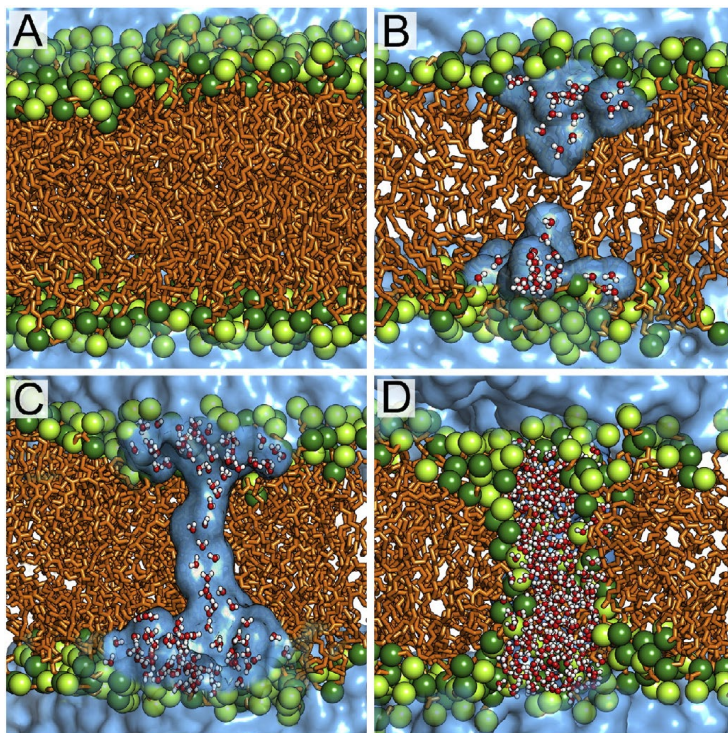


Figure 4 Pore formation model on the basis of ion imbalance. (A) Intact phospholipid membrane before pore formation. (B) Intrusion of water molecules from both sides of the membrane. (C) Formation of a water wire with hydrophobic tails lining the pore wall (hydrophobic pore, diameter <1 nm). (D) Expansion to larger hydrophilic pore (diameter ≥ 1 nm) with lipids rearranged for pore stabilization. From Kirsch and Böckmann, *Biochimica et Biophysica Acta* 2016 [20]

the dose-dependency of electroporation, explaining why pulses must be of sufficient magnitude or duration to result in pore expansion. If the externally applied potential is large enough to induce a critical amount of membrane flux, pores may continue to expand to a point at which their closure is no longer energetically favored. The process becomes irreversible and leads to permanent cell disruption. Whether this occurs due to limitless expansion of a single defect or when the total flux reaches a critical magnitude remains a matter of debate.[21] Simulations of pore formation dynamics suggest that the majority ($>95\%$) of defects caused at the sides facing electrodes have radii of <1 nm but only contribute about a third of field induced conductance.[22] The average radius of larger pores is about 20 nm and can grow up to about 400 nm. It appears that pore quantity increases with pulse duration and exposure time

whereas pore size is governed by field magnitude.[23,24] The multifactorial steady-state of pore formation and -resealing constitutes both the complexity and utility of electroporation. Since a given set of experimental parameters will result in a distinct reversible or irreversible outcome, possible exploitations range from cell fusion and cargo delivery to overall cell disruption.[1,25]

1.4 Applications of electroporation

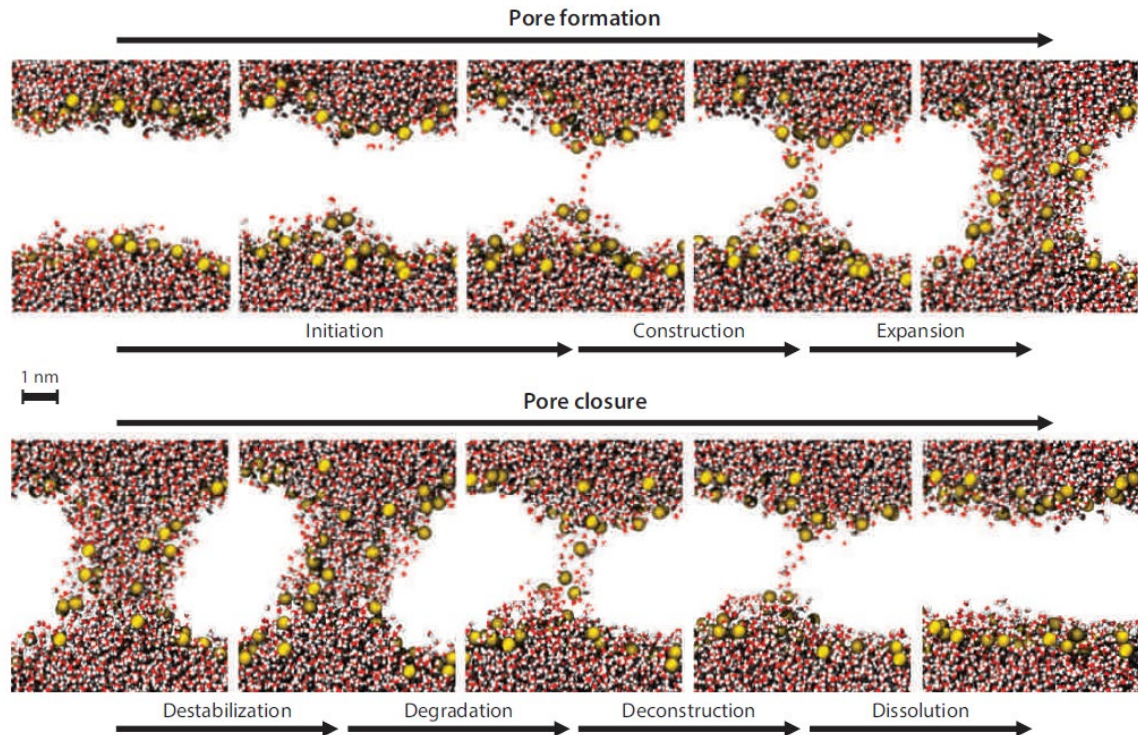


Figure 5 Current model of the dynamic formation and -closure of an electro-pore in a lipid bilayer. All stages are shown in order of appearance regardless of timescale. Pore formation processes assume an externally applied electric field and closure assumes that field application has ended. Lipid tails were removed for visual clarity. *Kotnik 2019 Membrane Electroporation and Electroporomeabilization – mechanisms and models* [25]

The following provides an overview of common implementations of irreversible and reversible electroporation in biotechnology. Cell disruption is achieved by increasing the electric field dosage to a point where pore expansion is irreversible. Increasing the dosage beyond this point will increase the likelihood of all sample material being affected, as is primarily desired for applications in the food industry.[26] Examples include bacterial inactivation, the harvesting of batch cultures or pre-processing of vegetable crops to reduce the energy requirements in downstream processing.[27] Unspecific side-effects of electric field application, such as electrochemistry and ohmic heating tend to promote the outcome and may be desired if product integrity is not compromised.[28] Lysis applications more relevant to this thesis require the introduction of a selective component that reduces the collateral impact of undesired, electrochemical reactions. One adaptation features the spatial arrangement of electrodes to focalize the electric field to a defined volume in solid tissues.[29] This is used for tumor ablation therapy, a medical application of electric fields that received FDA approval for the surgical ablation of soft tissue in 2008.[30] Since spatial field arrangement does not provide the same precision in a liquid suspension, selective lysis of cell suspensions tends to rely on the size specificity of electric fields implied in equation (1) to remove larger cell populations.[31–33] Details on this approach are provided in the second publication (Section 2.2).

A second class of electric field applications in biotechnology are based on reversible electroporation. One exploitation features the electrofusion of cells; a possible outcome of reversible pore formation induced by moderate electric field dosage is the fusion of two cell membranes to form a hybrid cell. [34,35] This method has been successfully employed to produce cells viable for cancer vaccine therapy.[36]

A more common application of reversible electroporation is the possibility of cargo delivery. This means that a compound added to the electroporation medium is transported through field-induced hydrophilic pores. The aim is for moderate field exposure to allow for pore resealing after electroporation, resulting in a large number of live cells that acquire the compound of interest. Studies on the delivery of small compounds such as Propidium Iodide have given critical experimental insights on the process of membrane electroporation.[37,38] The most common exploitation of reversible processes is termed calcium electroporation and relies on electroporation buffers with high calcium concentration that induce cellular apoptosis when uptake is facilitated via electric fields.[39] Essentially using a combination of electroporation and lysis, it offers the advantage that the lower electric fields necessary for reversible electroporation reduce collateral damage.[40] The local administration of chemotherapeutics such as bleomycin is a similar approach that can drastically reduce the systemic side effects of non-localized forms of drug administration (classic chemotherapy) while simultaneously facilitating transport to the target tissue.[41,42]

DNA delivery is a further, especially attractive exploitation of electroporation for two reasons. First, competing methods rely on either viral or chemical delivery and therefore necessarily contaminate the cell suspension with compounds that require later removal, while electric field treatment can be achieved without such contamination.[43] Second, experimental observations suggest that the impact of electric field exposure extends well beyond pore formation in the lipid bilayer.[44,45] Evidence for the field mediated induction of active DNA transport across the outer membrane and beyond appears to be conclusive, meaning that DNA-transfer may be achieved without any structural membrane damage.[46] While this explains the high survival rates of field-mediated transfection technologies, there is currently no satisfying hypothesis on how these differential processes are initiated by the exposure to external electric fields.

1.5 Current challenges

The pun of this chapter title is intended to emphasize the interaction between electrical energy and chemical change; electrolysis is a chemical reaction caused by an externally applied current. As introduced in section 1.1, electric fields in electroporation are the result of applying current to terminal electrodes. Terminal means that these electrodes are in contact with the liquid suspension – in this context referred to as the electroporation medium. Faraday's first law of electrolysis states that "The amount of chemical change during electrolysis is proportional to the charge passed".[47] Ohm's law further adds that current is directly proportional to the applied voltage, given by $I = U/R$. The reductionist implication of these relationships is that the amount of electrolysis accompanying electroporation is always proportional to the delivered dose of electrical energy. While this is a valid approximation for most of the discussed applications, many complex variables may impact the actual rate of electrolysis in a given system. One of these is electrolyte resistance, a crucial experimental parameter in electroporation. It is typically given as conductivity and depends on temperature, ionic concentration and -composition as well as the geometry of current distribution in the electrolyte.[48,49] Since boundary conditions where reduced conductivity increases electrolysis are

not encountered in electroporation,[50] we can state that the rate of electrolysis will be reduced in electroporation media of lower conductivity. This is both due to the increased resistance of the liquid - inversely proportional to current as per Ohm's law - but also because field and therefore current flow tends to be more uniform in low conducting liquids. [48,51,52]

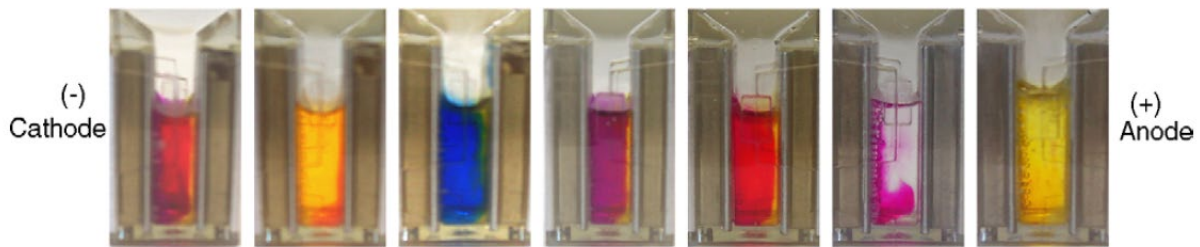


Figure 6 Indicator mediated detection of pH change as a result of electroporation-induced electrolysis in an aluminum electroporation cuvette of 4 mm electrode distance. Buffer resistivity: 568 Ω , electric field strength 45 kV m⁻¹, pulse duration 35 ms. Indicators left to right: cresol red, pH 0.2–1.8, red to yellow and pH 8.0–9.6, red to purple; methyl orange, pH 3.1–4.4, red to orange; bromocresol green, pH 3.8–5.4, yellow to blue; chlorophenol red, pH 4.8–6.4, yellow to violet; phenol red, pH 6.4–8.0, yellow to red; phenolphthalein, pH 8.0–9.6, colorless to red; alizarin yellow, pH 10.1–12.0, yellow to orange-red. *Kim Ja et al. 2008 Biosensors and Bioelectronics* [63]

A deeper understanding of the underlying phenomena requires an introduction to electrochemistry. Briefly, the kinetic equilibrium of electron transfer from one phase (electrode) to the other (liquid) or vice-versa depends on a compound's charge transfer resistance (CTR). It is expressed in Ohm and must be calculated for every individual compound that undergoes a kinetically controlled electrochemical reaction in the given system. In the following context, core features of this variable are; (1) that the total CTR will depend on the chemical composition of all phases and (2) that a higher CTR will result in reduced electron transfer and therefore electrolysis at the electrode-liquid interface.[53]

In determining the consequences of electrolysis, we will distinguish between reactions in the liquid and corrosion effects at the electrode. Electron transfer to and from the liquid causes pH change, gas formation (by water hydrolysis) and the formation of free radicals. Corrosion effects include electrode disintegration and the possible sedimentation of metal oxides depending on their composition.[54–56] The transformation of energy per se causes joule heating and, depending on potential, local arcing.[57] These unspecific side effects that accompany classic electroporation configurations negatively affect the outcome of field application in different ways: Large scale lysis or pre-processing systems in the food industry are primarily challenged by electrode disintegration when handling large volumes of substrate, meaning that treatment chambers must be replaced or serviced at regular intervals.[58] Meanwhile, chemical alterations to the substrate should be limited. Tumor ablation procedures struggle with collateral tissue damage as a result of local electrolysis.[59] Both in tissues and liquids, the theoretical potential of selectively disrupting larger cells as implied in the Schwan equation is not reflected in practice due to the unspecific nature of electrochemical side-effects.[60] Similarly, reversible electroporation applications suffer from viability loss due to either chemical lysis or local changes to the electroporation medium. The influence of temperature on the outcome of field exposure at constant settings confines many devices to a bulk configuration unless temperature stability can be ensured by external means.[61] These combined phenomena overshadow the potential biological specificity of electric field parameters in biotechnological applications.

Meanwhile, corrosion effects limit the usability of most commercial treatment chambers and essentially render them consumables that only deliver a reliable outcome at first use. This is of direct economic relevance to consumers of electroporation-based transfection technology, reflected in the

sale of one-time use electrode equipment by leading platform suppliers.[62] Notably, the same, leading technology remains a chemical transfection method with electric field-assisted plasmid entry. This simple fact serves to underline the notion that electroporation continues to suffer from a lack of reliability- and specificity. Therefore, competing technologies all share the ability to circumvent the impact of electrolysis in one way or another, as will be discussed in the following section.

1.6 Current remedies

Electrolysis is a consequence of charge transfer at the electrode-liquid interface and a primary challenge to most practical applications of electroporation.[63,64] Most remedies separately address the following three phenomena; Joule heating, electrode corrosion and chemical changes in the electroporation medium.

The necessity for temperature control is proportional to the number of pulses applied, as any fluctuations caused by the ongoing treatment will decrease the likelihood of a homogenous outcome. The biological impact of a given field strength depends on temperature and every additional pulse may itself cause an increase in temperature. This means that more susceptible cell populations will be over-proportionally affected as the treatment progresses.[61] Unless complete sample lysis is desired, this will result in an unpredictable practical outcome. Up to a certain volume, joule heating is sufficiently counteracted by surrounding the electroporation chamber with a cooling system.[31] More advanced technologies account for the successive temperature increase in flow-through devices, whereby the rate of cooling is increased toward the discharge site which has undergone more joule heating than the input end.[61] Electrode fouling and metal precipitation is highly dependent on electrode composition [54–56] and can be alleviated by the proper choice of material.[63] Platinum electrodes are far less prone to corrosion than gold or aluminum electrodes, and composite materials tailored for durability are increasingly common.[65,66]

The primary, biotechnological implications of charge transfer to- and from the electroporation buffer are pH change and gas formation. While most media are PBS-buffered, pH capacity has physiological restrictions and will not alleviate the significant, local pH-changes along the electrode interface. An innovative way to deal with gas formation and associated volume increase in flow systems is the use of flexible, porous materials at the non-electrode chamber walls.[67] Foamed polyethylene permits the passage of gas but not liquid and thereby continuously drains formed gases from the electroporation buffer.

Combining several individual remedies to electrolysis has enabled the commercialization of mammalian flow-through electroporation for small molecule delivery and transfection.[61] However, intellectual property reservations, product pricing and the complexity of device engineering render this approach unfit for the research sector. Competing technologies therefore strive toward a holistic approach to alleviate the consequences of electrolysis. One approach is to increase the frequency to the megahertz range. The resulting pulses have nanosecond (ns) period, which is shorter than the rate of electrolysis reactions. With this method, the second term of the Schwan equation significantly contributes to the change in membrane potential. Therefore, responses to ns electroporation give rise to entirely different phenomena and dependencies such as organelle permeabilization and the direct manipulation of protein activity.[10,68] This effectively makes ns- electroporation a separate field in terms of electroporation mechanics. The most common strategy to remedy electrolysis in settings using longer pulses takes advantage of the fact that charge transfer is confined to the interface; increasing electrode distance can ensure that cell suspensions are spatially separated from electrodes. [63,69,70] This inevitably increases the potentials necessary to reach sufficient, local field magnitudes. However, chamber geometries can be designed to allow for focal concentration of inhomogeneous fields towards an area or section of choice.[70] A further, inherently different strategy is to increase

the charge transfer resistance along the interface to a point where energy conversion is inhibited. This concept is the technological basis of this thesis and will be detailed in the following section.

1.7 Capacitive coupling

A capacitor is a component with the ability to store electrical energy. A basic configuration would consist of two conductive materials (i.e. metal plates) that are electrically separated, which is given if the dividing space consists of highly insulating dielectric such as air, plastic or ceramic. When current is applied, electrons may flow onto the metal plates until the voltage difference between them equals the voltage applied to the circuit. As a result, electrical energy is stored in the form of an electric field that exerts a force on the bridging dielectric. A materials capacitance (C) describes the magnitude of charge it can store per unit potential. This measurable quantity depends on the degree to which the material can be polarized at the given voltage and is termed the absolute permittivity (ϵ) of the respective dielectric. It is more commonly summarized as the dielectric constant (k); the factor by which the material increases the capacitance compared to the same volume of air. The total capacitance of a capacitor is further determined by the thickness of the dielectric (d) and the surface of electrode contact (A), yielding $C = \epsilon(A/d)$. As a deliberately reductionist conclusion that restricts the

spectrum of critical variables to a relevant contextual range; the suitability of a certain dielectric to yield a large capacity per volume is denoted by its dielectric constant. The term high- k electrode coating in the context of this thesis refers to a dielectric constant larger than 3,9. This simply describes a material that stores a relatively large amount of electric energy per given volume, and one of the two key features of what

we term electrode passivation.[4,71] In engineering terms, coating electrodes with a high- k material is the only distinguishing feature of a passivated electroporation chamber. However, the implications of this coating result in considerable complexity; since the terminal electrodes are flanked by high- k material and these are in turn separated by the electroporation buffer, even a cell-free configuration essentially consists of three dielectric layers. While the layer with the highest dielectric constant is readily polarized and thereby stores the largest amount of coulomb per voltage, the layer with the lowest dielectric constant will show relatively greater resistance to polarization that results in a higher voltage drop and therefore a higher electric field.[72] The high- k material used in the following publications, Titanium Dioxide, has a dielectric constant between 60 [73] and 85 [74] (depending on crystal structure that arises by formation method and -settings). The significance of this is understood when learning that water has a similarly large dielectric constant close to 80 and that the addition of ionic solvents in the physiological range have no pronounced impact on this property.[75] Because both components have similar permittivity, the electric field acting on the dielectric coating and the electroporation buffer will also have similar magnitude. Using a thin high- k dielectric passivation layer in the nm-range thereby ensures that the potential drop occurs predominantly in the much larger volume of electroporation buffer.

The second key property of the insulating material is electrical breakdown resistance. All insulating materials have an inherent breakdown voltage which indicates the electric potential per material thickness at which it becomes conductive. For Titanium Dioxide, literature values range between 2.7 MV/cm [76] and 27 MV/cm [77], meaning that electric field strengths common in electroporation

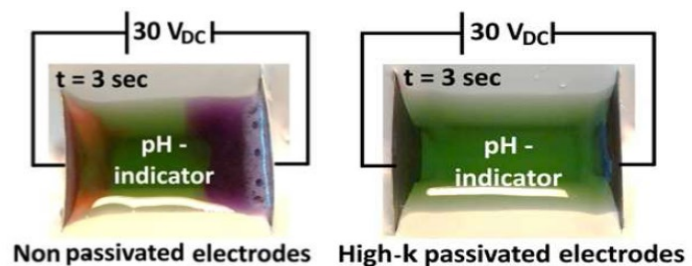


Figure 7 Interfacial pH change as a result of applying 30 V_{DC} to terminal electrodes with- and without high- k passivation. Wassermann 2016 *Applied Materials & Interfaces* [71]

(kV/cm range) would be enabled by a passivation thickness in the lower μm -range for an electrode gap of 1 cm. This explains why a layer-thickness in the nm-range is sufficient for the microfluidic applications (gap = 81.3 μm) featured in this thesis.

Note that both the dielectric constant and breakdown resistance of a material are in fact complex properties that will depend on temperature, frequency, molecular composition and crystal structure among further variables.[78] Given that the operating conditions in the following publications feature relatively constant buffer composition, low frequencies and standardized passivation protocols, we can assume the relative material characteristics to resemble the static values presented above.

One last dimension that is crucial to understanding the different mechanisms of capacitively coupled electroporation as opposed to standard ohmic coupling, is the time-resolved reaction of an ionic solution exposed to an external electric field. In the corresponding resting state, ions will be randomly distributed throughout the solution unless they are associated with polarized surfaces in the form of double layers. An applied potential will result in ionic movement toward electrodes of opposing charge regardless of the configuration. The rate of charge separation depends on electric field intensity and ionic mobility, resulting in typical drift velocities of tens of microns per second for small ions subjected to 1 V/m.[79] Remembering that the potential drop and therefore electric field is largest where force is exerted, successive ion accumulation at the electrode surface will increase the potential drop near the interface and thereby reduce the electric field acting in the bulk of the liquid.[80] In a typical, ohmic configuration, electrochemistry counteracts this phenomenon, as charge transfer leads to the formation of reversely charged ions that will drift toward the opposing electrode. At equilibrium, ionic movement in the bulk solution sustains an electric field that will be proportional to the measured current which in turn reflects the magnitude of charge transfer.[81] This steady state is responsible for the significance of pulse duration in ohmic coupling. For passivated electrodes, sustained ion mobility is inhibited by the increased charge transfer resistance at the interface. Charge separation will therefore successively confine the potential drop to the electrode interface and reduce electric field effects in the bulk solution. This means that there is no electric field acting on a cell suspension in equilibrium, which is reached when the electrodes reach their maximum potential.

2. Publications

2.1 Controllable cell manipulation in a microfluidic pipette-tip design using capacitive coupling of electric fields

Authors

Terje Wimberger,^{ab} Johannes R. Peham,^a Eva-Kathrin Ehmoser^b and Klemens J. Wassermann^a

Affiliations

^a Austrian Institute of Technology GmbH, Department for Health & Bioresources, Vienna, Austria

^b University of Natural Resources and Life Sciences, Department for Nanobiotechnology, Vienna, Austria

Author contributions

TW, JRP, EKE and KJW are responsible for conceptualization of the idea. **TW** conducted data curation and formal analysis. KJW is responsible for funding acquisition. **TW** is responsible for investigation and specifically performed experiments and data acquisition. **TW**, EKE and KJW developed the methodology. EKE and KJW are responsible for administration, resources and supervision. **TW** is responsible for validation. **TW**, JRP, EKE and KJW are responsible for visualization, preparation, creation and presentation of the published work. **TW** wrote the original draft. **TW**, JRP, EKE and KJW are responsible for review and editing. All authors have read and approved the manuscript.




Author comment

As the outset of this thesis, high-k coated electrodes had never been used to treat mammalian culture cells. The primary goal was to develop a protocol for cell transfection that could compete with current field-mediated gene delivery standards in terms of efficiency and viability, while offering superior usability through device miniaturization. At the time, the only existing design consisted of a flow-through configuration that will be introduced in the second publication. It was decided to devise an adaptation that would relieve the platform of dead volume so that a single parameter test would consume a minimal amount of plasmid. The configuration presented in this publication is the result of these efforts, featuring a reusable pipette tip with a microfluidic channel of 10 μ l sandwiched between a pair of passivated electrodes. Early attempts mimicking existing electroporation buffers and field exposure parameters from literature showed highly ambiguous results. The core discovery that enabled a reproducible outcome was the requirement to lower buffer conductivity to the μ S/cm range, orders of magnitude lower than standard electroporation buffers. Though consistent, subsequent attempts to replicate cell permeabilization- or transfection experiments from pertinent literature remained unsuccessful. It was concluded that previously published field parameters for cell manipulation do not readily translate to configuration with high-k coated electrodes, stressing the need to recharacterize the impact of classic variables such as field strength, conductivity, pulse number and frequency for the platform at hand. The following publication provides precise descriptions of the interdependencies between exposure parameters within their respective, relevant range. This knowledge enabled the successful transfection of 293T cells by adapting the shape of the delivery pulse to introduce an electrophoretic component to the treatment.



Cite this: *Lab Chip*, 2019, 19, 3997

Controllable cell manipulation in a microfluidic pipette-tip design using capacitive coupling of electric fields

Terje Wimberger, ^{*ab} Johannes R. Peham,^a
 Eva-Kathrin Ehmoser ^b and Klemens J. Wassermann ^{*a}

Systems designed toward cell manipulation by electric fields are inherently challenged by energy dissipation along the electrode–electrolyte interface. A promising remedy is the introduction of high-*k* electrode passivation, enabling efficient capacitive coupling of electric fields into biological samples. We present the implementation of this strategy in a reusable pipette tip design featuring a 10 μL chamber volume for life science applications. Prototype validation and comparison to conductive gold-coated electrodes reveal a consistent and controllable biological effect that significantly increases the reproducibility of lysis events. The system provides precise descriptions of HEK-293 lysis dependency to variables such as field strength, frequency, and conductivity. Over 80% of cells were reversibly electroporated with minimal electrical lysis over a broad range of field settings. Successful transfection requires exponential decay pulses and showcases how modulating capacitive coupling can advance our understanding of fundamental mechanics in the field of electroporation.

Received 18th September 2019,
 Accepted 20th September 2019

DOI: 10.1039/c9lc00927b

rsc.li/loc

Introduction

Electroporation describes the use of electric fields towards alteration of biological cells and tissues.¹ Depending on field parameters, the subjected cells undergo changes in size, shape and membrane uniformity.^{2,3} While high electric fields lead to cell lysis (irreversible electroporation), applying moderate fields yield a reversible, non-lethal response that can be used for cell fusion or cargo delivery.⁴ The latter technique is utilized in a wide range of medical and research applications, ranging from gene delivery and stem cell isolation to electro-chemotherapy.⁵ In comparison to viral and chemical approaches for cargo- or gene transfer, electroporation has several advantages such as adaptability, high transfection rate, absence of contaminants and low immunogenicity.^{6,7} In practice, one of the biggest challenges in electroporation is the limited precision of the effect which reduces cell survival or causes collateral tissue damage.^{8,9}

The causative effect of cellular damage is the result of various electrolytic processes that occur at the electrode interface.¹⁰ Unwanted side-effects include joule heating, pH change, bubble formation and electrode disintegration.^{8,11,12}

Gases formed at the solution boundary may become ionized with continuing exposure to high electric fields which in turn leads to arcing and high local temperature increase.¹¹ In sum, classic electric field application systems using metallic electrodes in direct contact with an electrolyte are always accompanied by varying degrees of adverse and unspecific side-effects which reduce cell survival, analyte integrity, reproducibility and the lifetime of electrodes.¹³

Several innovative attempts have been made to tackle this issue. Approaches include the spatial separation of electrodes and cells,⁸ fast reversal of electrochemical reactions by high frequency alternating currents¹⁴ and the introduction of nanosecond-timescale electroporation. The latter turns out to exemplify a special case for electroporation, with smaller pore sizes and substantially different effects such as organelle specificity.¹⁵ However, all three approaches require highly specialized electronic equipment regardless of their application.

Microfluidic approaches that aim to alleviate the adverse effects of electrolysis do so with varying degrees of success; persisting issues include loss of field uniformity due to complex electrode or fluidic channel geometries, elaborate flow concepts causing cell deformation and low throughput in highly miniaturized systems.^{16,17} As authors and reviewers of such platforms point out, the major problem facing novel electroporation systems might be traced back to a persisting lack of mechanistic knowledge about the electroporation process itself.^{18,19}

^a Austrian Institute of Technology GmbH, Department for Health & Bioresources, Vienna, Austria. E-mail: Terje.wimberger@ait.ac.at, Klemens.wassermann@ait.ac.at

^b University of Natural Resources and Life Sciences, Department for Nanobiotechnology, Vienna, Austria



This study presents an attractive alternative to the above-mentioned adaptations by implementing electrodes insulated with a dielectric passivation layer. Foremost, this allows us to investigate isolated electric field effects by suppressing secondary effects that are the result of faradaic current.^{20,21} The outcome is equally effective and resolves issues like electrolysis, pH change and electrode disintegration by limiting electrochemistry along the electrode interface. At the same time, the required electronic setup for pulse delivery remains simple. An efficient ohmic decoupling of electrode and liquid was previously utilized towards selective lysis of blood cells for sample preparation in a sepsis model.²¹ The TiO₂ passivation forms a biocompatible, chemically inert layer with a high dielectric constant ($\epsilon_r > 60$) which is generated by thermal oxidation of titanium electrodes. This high-*k* coating design enables efficient capacitive coupling of the electric field into the liquid.

Capacitive coupling has a history of use in contactless dielectrophoresis, where it has successfully resolved issues associated with electrode fouling during continuous low-energy field application at high frequencies.^{22,23} Here, the impact dielectric electrode coating on mammalian culture cells was assessed by lysis experiments with HEK-293 cells. Important known variables such as field strength, solution conductivity, pulse frequency and -number are addressed.

A window of opportunity exists between the pulse-field magnitude required for reversible and irreversible electroporation.^{24,25} A highly specific field effect is desired for a homogeneous cell population such that a high fraction of cells are reversibly permeabilized without significant lysis. HEK-293 permeabilization experiments with propidium iodide (PI) showcase the specificity of high-*k* passivation by offering multiple settings to match these criteria. Subsequent experiments show that knowledge of efficient permeabilization settings can be used toward transfection of HEK-293 cells.

A further aim is to demonstrate the versatility of the material by complementing the existing flow-through design²¹ through a stationary, microfluidic pipette tip. By adapting the electric cell lysis unit (ECLU) into such a pipette tip design we present a convenient, low-throughput device optimized for life science applications. Given the small electrode distance of 81.3 μm , a battery driven version of the electroporation pipette can be envisioned for flexible and cost-effective use.

Materials and methods

Production of titanium-oxide coated prototypes

Grade 2 titanium foil (commercially pure titanium, cpTi with a purity of 99.2%) was cut in dimensions of 60 \times 10 mm. Electrodes were cleaned and coated with titanium dioxide for an average thickness of 600 nm according to an optimized passivation procedure.²¹ Briefly, titanium sheets were cleaned with a series of acetone, ddH₂O and 2-propanol washes in an ultrasonic bath for 20 minutes each. Clean sheets were

transferred to a muffle furnace (L 9/11P330, Schaefer & Lehmann, Germany) for thermal oxidation at 650 $^{\circ}\text{C}$. Rise time was 2 hours and the maximum temperature sustained for 3 hours before passive cooling to room temperature.

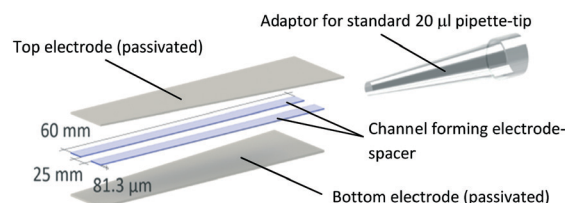
Electroporation reservoirs were assembled using a double sided adhesive tape with defined thickness and biocompatibility²⁶ (Adhesive Research, Arcare 90445). It provides a vertical spacing of 81.3 μm , placed 2.5 mm apart forming a channel with a volume of 12.15 μl (Scheme 1). The top 5 mm of a standard 20 μl pipette tip were removed and a short, 90 $^{\circ}$ incision was made in the resulting narrow end. Electroporation tip assembly proceeded by inserting the electrode-flanked channel into the incision and sealing any edges air-tight with two-component epoxy adhesive (UHU plus Endfest 300, 45 640). The resulting tips can be used with any 20 μl pipette, set to a volume of 10 μl .

Production of gold coated prototypes

Rinsed titanium electrodes were coated with 60 nm Gold upon an adhesive layer of chrome (2–3 nm) using a vacuum coating system (Lab Coater Auto 306 with FL400 loading box, HHV). Prototype assembly was performed as described in the previous section.

Cyclic voltammetry

Buffers were prepared by dilution of PBS with Milli-Q water (Sartorius, 18 MOhm cm^{-1}) by 1:10 and 1:100. D-Sucrose (Fisher BioReagents, BP220-10) was dissolved in ddH₂O to yield a 250 mM stock solution. The buffers were aspirated into gold or titanium oxide prototype tips and connected to the impedance analyser (Metrohm Autolab B.V., $\mu\text{AUTOLAB III/FRA2}$) without reference electrode. Three cycles of current measurements were performed for voltages between +5 V_{DC} and –5 V_{DC} for all buffers and prototypes with a scan rate of 0.05 V s^{–1} and step resolution of 2 mV. Titanium oxide coated electrode measurements include values for air (unfilled).



Scheme 1 Prototype design and dimensions of the electroporation pipette tip. A microfluidic channel forms between the passivated titanium sheets shown on the top and bottom and flanked by double-sided adhesive tape, resulting in a channel volume of 12.15 μl . The top end of the channel was sealed to a standard 20 μl pipette-tip. With this adaptor, the channel acts as an elongation of the pipette tip and liquid can be aspirated via the open end of the channel. Images of an actual prototype are shown in Fig. 2 of the results section.



Leakage current measurements

Titanium oxide coated prototype tips were filled with PBS and electrodes connected to DC power supply (DP832, Rigol), and a multimeter (Fluke 289) in series. DC voltages of 5, 10, 15, 20, 25 and 30 V were applied *via* the DC power supply and the corresponding currents were measured by the multimeter.

Cell culture

Human embryonic kidney cells (HEK-293; ATCC CRL-1573) were cultivated at 37 °C and 5% CO₂ in DMEM (Thermo Fisher, 41965) supplemented with 10% FBS (Thermo Fisher, 10500) and 1% Pen/Strep Antibiotic-Antimycotic (Thermo Fisher, 15240). Cells were passaged by washing with PBS (1× from stock: Thermo Fisher, 70011044) followed by trypsinization (0.25%, Thermo Fisher, 25200) for 5 min at 37 °C and reconstituted in culture Medium. Any sterile protocols were processed in biological safety cabinets (Herasafe KS, Class II, Thermo Fisher, 51022488).

Sample preparation

Cells were washed with PBS, detached by trypsinization and resuspended in supplemented DMEM medium. Electroporation buffer (EPB) was prepared from autoclaved 250 mM sucrose solution. PBS was added to adjust the desired sample conductivity, which was measured using a conductivity meter (B-771 LAQUAtwin, HORIBA Advanced Techno). Cells were centrifuged for 5 min at 400 g (RT), supernatant discarded and resuspended with EPB. After two washing steps, cells were counted and adjusted to 10⁶ cells per ml with the next reconstitution. Final conductivity was recorded. If the suspension deviated more than 10 μS cm⁻¹ from the calibrated EPB, the washing step was repeated until conductivity was within this range. Cell death from sample preparation was also assessed. Only samples containing more than 85% live cells as determined by Hoechst 33342 stain were used for experiments.

Electroporation and imaging

HEK-293 cell lysis was used as a readout to analyze the biological impact of capacitive coupled electric fields on cells. Suspension of cells in EP buffer were transferred to hydrophobic parafilm in 10 μl droplets and aspirated with the electroporation tip. Electric fields were induced by applying the respective waveforms with a function generator (DG4102, Rigol) connected to a voltage amplifier (Falco WMA-300, Falco Systems, Netherlands). Voltages and currents were monitored (*via* a 2 Ω resistor) by an oscilloscope (DS1104B, Rigol). All indicated voltages refer to the maximum potential at the electrodes after capacitive charging is complete. When indicated, the conjectural field strength is derived by $U/d = E$. Both quantities refer to theoretical maxima that are proportional, but not equal to the effective electric field inside the electroporated medium.

After field application, cells were ejected onto parafilm and mixed with a 10 μg ml⁻¹ (10×) stock solution of Hoechst 33342 in PBS for a final concentration of 1 μg ml⁻¹. The sample was transferred to a hemocytometer (Thoma, Optik Labor) and imaged by a digital camera (Prosilica GT, Allied Vision) mounted on an inverted microscope (CKX41 Fluo V2, Olympus). Imaging in the hemocytometer ensures that each picture represents an equal volume of cell suspension. Bright-field images were recorded for total cell count. To identify lysed cells, Hoechst 33342 viability dye was excited at 360 nm using a UV light-source (X-Cite 120Q, Excelitas Technologies) and emission above 420 nm imaged for further analysis.

For permeabilization experiments, the cell suspension was mixed 1:10 with a 30 μg μl⁻¹ solution of propidium iodide prior to field exposure. The dye was prepared from dilution of a 1 mg ml⁻¹ stock with electroporation buffer to limit any conductivity change. As previously, the suspension was aspirated in the prototype channel and pulses were applied *via* the connected function generator. After field application, cells were directly ejected to the hemocytometer. To identify permeabilized cells, the membrane impermeable PI was excited from 480–550 nm using a UV light-source (X-Cite 120Q, Excelitas Technologies) and emission above 590 nm imaged for further analysis.

Data analysis

Lysis images were analyzed in Fiji²⁷ by adjusting the threshold to include positive cells only, isolating high-contrast live cells in bright-field and stained dead cells in fluorescence images. After converting images to binary, cell count was performed by the particle analysis function.

Results are displayed as percentage lysed, excluding the fraction of dead cells from sample preparation, which means that the control is always displayed as zero percent lysis.

PI-positive cells were counted manually from a bright-field and red fluorescence overlay. Controls were overexposed to the point where PI-negative cells remain invisible. This setting was then applied to samples subjected to electric fields. Dead cells show high-PI fluorescence, deformed or disintegrated structure in bright-field and were calculated equally as in lysis experiments. Permeabilized cells are displayed as the fraction of visibly live cells with PI fluorescence.

Transfection

Transfection requires cancellation of the inherent negative charge of the DNA molecule to allow for the formation of stable membrane-DNA complexes. This is most commonly achieved by the addition of MgCl₂ as described in the majority of standard electro-transfection protocols.²⁸ HEK-293 cells were prepared as for lysis experiments and kept in a sterile working environment. 9 μl of cell suspension was placed on hydrophobic parafilm and mixed with 1 μl vector stock solution for a final working concentration of 25 ng ml⁻¹



pTurboRFP-N (Evrogen, FP232) and 0.5 mM MgCl_2 . The suspension was aspirated into the electroporation tip and exposed to 10 square wave or exponential decay pulses of 40 V at 1 kHz. They were ejected into an 8-well μ -slide (Ibidi, 80826) and left to rest for 5 minutes. 250 μl OptiMEM (Thermo Fischer, 31985062) was added with gentle resuspension. Transfected cells were cultivated at 37 °C and 5% CO_2 for 48 hours and imaged by a digital camera (Prosilica GT, Allied Vision) mounted on an inverted microscope (CKX41 Fluo V2, Olympus). The fraction of cells expressing RFP was assessed from manual count of bright-field and red fluorescence overlays of at least 5 images from random positions in each respective well.

Statistics

Where applicable, n refers to the number of technical replicates with the same cell suspension and prototype. Each replicate consists of 3 imaging-replicates for lysis experiments and 5 imaging-replicates for permeabilization and transfection experiments. As such, any data point concerning lysis shows mean and standard deviation (SD) of 3 data points, in turn based upon 9 separately analysed microscopy images.

Where stated, Pearson correlation was computed between both data sets. Coefficients of variation for four different prototypes refer to the ratio of the SD to the mean. In the final section, p value was calculated using unpaired, parametric t -test (two-tailed) with Welch's correction since equal SD cannot be assumed for the different pulses applied.

Results and discussion

Electrochemical implications of high- k electrode passivation

The introduction of an electrically insulating passivation leads to an ohmic decoupling of the electrode material from the liquid, limiting secondary effects of faradaic current acting on the electrolyte. This section demonstrates the advantages of using ohmic decoupling of the electrodes as compared to non-decoupled electrodes with respect to electrochemical reactions at the electrode-electrolyte interface.

Fig. 1 quantifies passivation efficiency of the metal oxide layer for different buffer conductivities. Electrodes with 60 nm Au coating reveal the faradaic current equivalents of a non-insulated system representing a standard electroporation setup. Fig. 1a shows current measurements with gold-coated titanium electrodes for potentials between -5 and 5 V_{DC} . Signal spikes are indicative of electrochemical reactions. Readings for higher conductivities were increasingly erratic above 4 V_{DC} , peaking between 2 mA and 9 mA. Electrode passivation significantly reduces the amount of current by approximately 4 orders of magnitude for all buffer dilutions (Fig. 1b). Passivated electrodes show no significant dependency on solution conductivity, as different PBS dilutions have similar current responses and peak around 2 μA . Measurements for empty electrodes (air filled) confirm that leakage current does not pass through the adhesive and

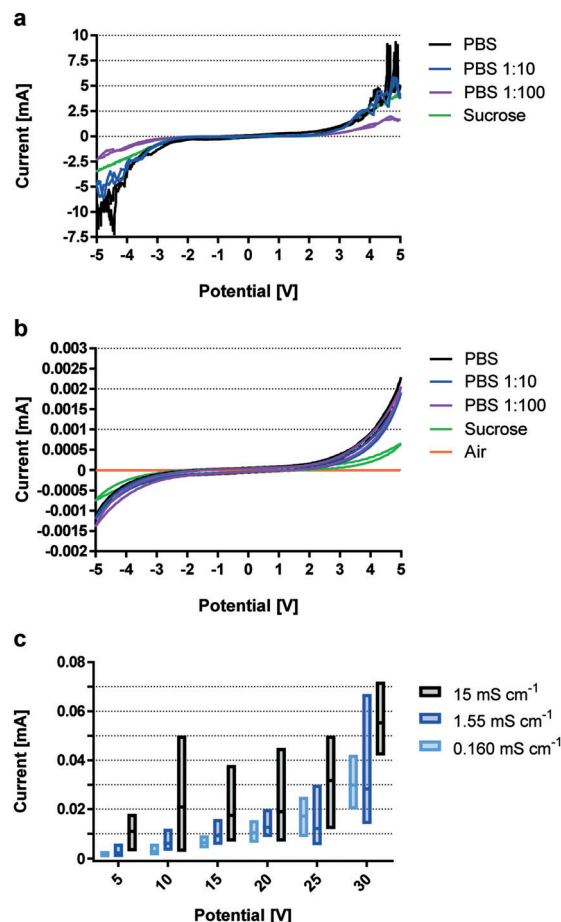


Fig. 1 Quantification of passivation efficiency in terms of current flow. Leakage current between $+5$ V_{DC} and -5 V_{DC} for pipette tip prototypes constructed with Au electrodes (a) and TiO_x passivated electrodes (b and c), where c) shows results for voltages between 5 V_{DC} and 30 V_{DC} . $n = 1$ with 3 measurements.

was recorded at 20 nA. Due to the voltage limit of the impedance analyzer higher voltages were analyzed using a DC power source.

Fig. 1c shows leakage currents for passivated electrodes, which remain below 10^{-4} A for all conductivities and voltages up to 30 V_{DC} . While currents for buffer conductivities of 0.160 mS cm^{-1} and 1.55 mS cm^{-1} remain similar, readings for 15 mS cm^{-1} were consistently higher. Most notably, SD increased with conductivity and applied voltage, but never exceeded 72 μA even when using a highly conductive solution and 30 V_{DC} .

By minimizing the superimposing effects of faradaic current and thereby electrochemical reactions, high- k materials have great potential for highly reproducible and defined cell manipulation by electrical fields in microfluidic devices.

Characterization of electrode pipette tips

High- k materials such as titanium dioxide successfully allow for ohmic decoupling of electrode interfaces from the



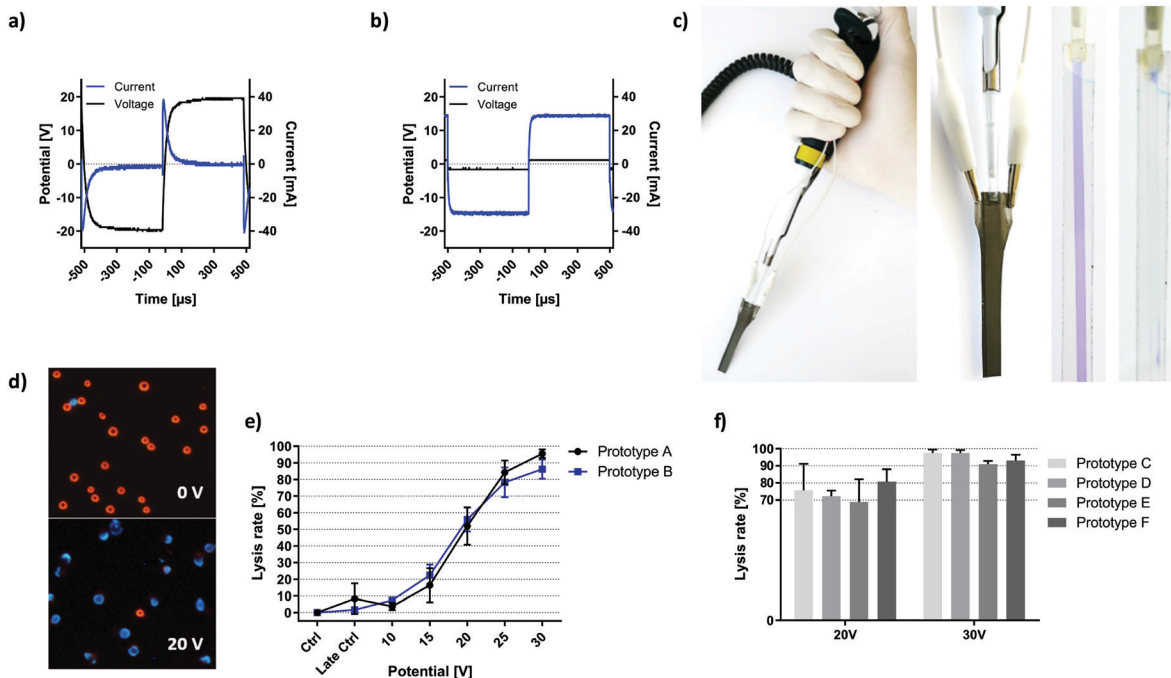


Fig. 2 Prototype description and validation. Voltage and current characteristics of prototypes using a) passivated and b) unpassivated electrodes when 20 V were applied to a PBS-filled channel at 1 kHz. c) Images of the prototype incorporated in a regular pipette configuration. Each respective electrode was contacted *via* alligator clamps. A flexible 2-pole cable connects the device to an amplified function generator. Transparent versions of the prototype visualize the microfluidic properties of the prototype channel. d) Overlay-image showing live (red) and dead (blue) cells at 0 V and 20 V with 6000 square waves applied at 1 kHz. Brightness and contrast have been enhanced for better visualization. e) Field dependency of HEK-293 cell lysis with two different prototypes. $f = 1$ kHz, $\sigma = 260 \mu\text{S cm}^{-1}$, exposure = 10 seconds, $n = 3$, error bars = SD. f) HEK-293 cell lysis at given voltage performed with 4 further prototypes. $f = 1$ kHz, $\sigma = 160\text{--}171 \mu\text{S cm}^{-1}$, exposure = 6 seconds, $n = 3$.

solution while efficient coupling of the electric field is enabled by its low capacitive reactance.

Fig. 2a and b compare the voltage and current characteristics upon application of a 20 V, 1 kHz square AC signal to a PBS-filled channel comprising Au or TiO_2 covered titanium electrodes, respectively. For the conductive Au coating, continuous current flow through the solution was observed due to direct contact between electrode material and the solution. In the case of TiO_2 -coated electrodes, current flow is restricted to an initial capacitive charging of electrodes which stops when the set potential is reached, and no dynamic voltage change occurs ($dU/dt = 0$). This is a consequence of ohmic decoupling, the efficiency of which was quantified in detail in the previous section.

Fig. 2c shows the pipette with the electrode tip in working configuration. Electrodes were connected to the circuit *via* the upper lugs where the passivation layer was removed.

The channel was visualized using a blue dye in a transparent fluidic demonstrator (without the optically intransparent electrodes). The fluidic compartment was bonded to a standard pipette tip, which acted as an adapter between microfluidics and any 20 μL pipette.

Fig. 2d shows images of HEK cells without treatment and upon electric field exposure at lysis settings. Live cells are visible in the bright-field channel (visualized as red) and Hoechst 33342 viability stain shows dead cells visible in the blue channel.

To assess the reliability of prototype production, individual cell lysis curves were recorded with 6 functional electroporation pipette tips (passivated) with lysis triplicates. Fig. 2e shows lysis behaviour of HEK-293 cells exposed to 10 seconds of square wave signals with respective magnitude. The only variable was the prototype tip used. All data was standardized to the early control such that cell death from the preparation procedure was neglected in lysis values. Late control shows electric-field independent HEK-293 cell death over the course of respective experiments. Except for the data points at 30 V, all plotted values for one prototype fall within the SD of the other with a Pearson correlation of $r^2 = 0.9817$. SD is 5.5% for prototype A and 4.8% for prototype B. The highest SD was observed in the dynamic range of cell lysis (15–25 V). Similarly, Fig. 2f compares four different prototypes with respect to HEK-293 cell lysis upon 6 seconds of square wave exposure at the indicated voltage and lower solution conductivity. Application of 20 V resulted in 74.4% lysis with a combined SD of 10.0%. For individual prototypes, coefficients of variation range between 4.6% (prototype D) and 20.6% (prototype C). At 30 V lysis results were increasingly consistent, where the lysis rate of 94.7% deviated by 3.4% in total. Coefficients of variation range between 1.8% (prototype D) and 3.8% (prototype F).

The high consistency of recorded lysis events is surprising, given that sources of deviation include all passivation- and construction steps as well as randomized errors from the



chosen readout. Most importantly, prototype construction is highly precise and does not represent a source of directed error in terms of HEK-293 cell lysis. This is the key prerequisite for identification of relevant lysis parameters in subsequent experiments.

Capacitive coupling dynamics are highly sensitive to cell suspension conductivity

We proceed to show the effects of electrode coating in terms of biological impact by presenting HEK-293 cell lysis dynamics at varying field strengths and buffer conductivities. Previous publications that have investigated the biological impact of solution conductivity have found contradicting correlations with respect to cell survival in response to electroporation. One study reports that lower conductivity promotes survival of DC3F cells when investigating the range between 0.01 to 10 mS cm⁻¹.²⁹ Another study finds increased survival of murine myeloma cells with increased buffer conductivity in the more narrow range between 0.8 and 3.7 mS cm⁻¹.³⁰ However, neither of the studies used a passivated or microfluidic setup and the tested conductivities included much larger changes or fall into a different range than the comparably minor changes of ± 0.1 mS cm⁻¹ between 0.06 and 0.26 mS cm⁻¹ addressed here.

For mammalian cells, the threshold for low frequency electroporation is generally considered as 1 kV cm⁻¹.^{7,31} Using gold-coated electrodes, onset of HEK-293 cell lysis (16.3–30.8%) was observed at 0.617 kV cm⁻¹ (Fig. 3a).

Large variations for cell lysis with gold electrodes are the result of the multi-factorial nature of the lysis effect (electric field, electrolysis, electrochemistry, pH and temperature). The drawback of this combination was made clear by the difference in SD between gold and titanium oxide coated prototypes (Fig. 3a and b). The lack of reproducibility for gold electrodes was likely caused by the small electrode distance in the prototype channel. Any electrolytic activity as the result of an applied voltage will have random local distribution, thus making the fraction of affected cells unpredictable. There was no clear correlation between buffer conductivity and average cell lysis using gold-coated electrodes in this configuration.

In contrast, lysis curves for different conductivities remain distinctly separated when applying capacitively coupled electric fields (Fig. 3b). For a conductivity of 60 μ S cm⁻¹, lysis began at 1.2 kV cm⁻¹ and reached a plateau at 2.4 kV cm⁻¹. Increasing the conductivity to 160 μ S cm⁻¹, we observed lysis starting below 1.8 kV cm⁻¹ and peaking at 3 kV cm⁻¹. With 260 μ S cm⁻¹, onset of lysis occurred at 2.4 kV cm⁻¹ and reached its maximum around 3.6 kV cm⁻¹. In sum, the lysis efficiency of HEK-293 cells was inversely proportional to buffer conductivity. This trend was highly reproducible and lysis curves are clearly distinguished by minor changes in buffer composition. The increase in the necessary field strength for cell lysis in the passivated electrode setup compared to gold electrodes was caused by a potential drop inside the passivation layer. However, due to the microfluidic setup and the high-*k* nature of the passivation material, high electric field-mediated lysis efficiency was reached at low voltage amplitudes. Solution conductivity must be sufficiently low for the applied voltages to influence HEK-293 cell viability. The steep correlation between lower conductivity and an increase in lysis efficiency can be attributed to ionic losses. As shown in a theoretical study of a similar system, current density is reduced by an increase in conductivity and leads to a faster decay of the electric field.¹¹

AC lysis efficiency is independent of square wave frequency and determined by pulse number

Fig. 4a shows HEK-293 cell lysis upon 6 second exposure to electric fields of rising magnitude applied by capacitive coupling. In all following descriptions, one pulse refers to a full AC square wave period. Pulses were applied in the same buffer at frequencies ranging from 50 Hz to 1 kHz. The data suggest that lysis efficiency positively correlates with both field strength and AC frequency. Because buffer conductivities were constant (165 ± 5 μ S cm⁻¹), onset of lysis was observed from 1.8 kV cm⁻¹ in all cases. However, given that the total time that cells were exposed to the electric field was equal (6 seconds), the number of pulses increases with frequency. To distinguish frequency dependency from the impact of overall pulse number, total field exposure time was

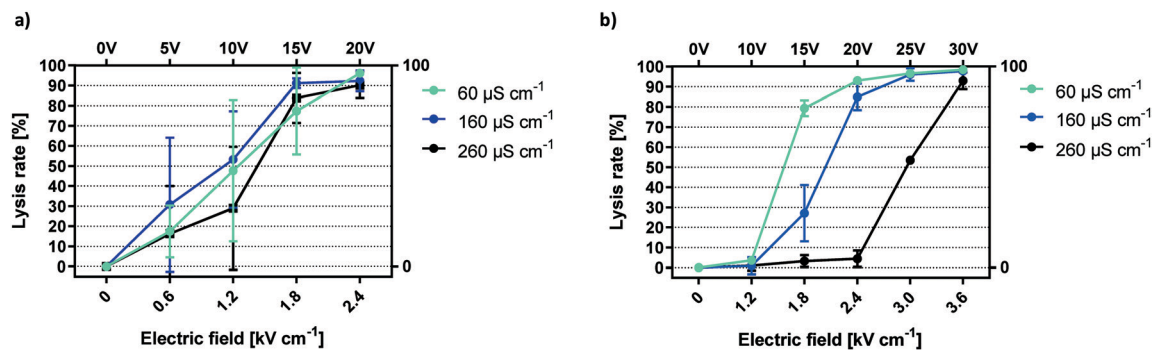
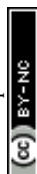


Fig. 3 Conductivity dependency of electric field mediated lysis. Lysis efficiencies for HEK-293 cells using unpassivated a) and passivated electrodes b). $f = 1$ kHz, exposure = 6 seconds, $n = 3$.



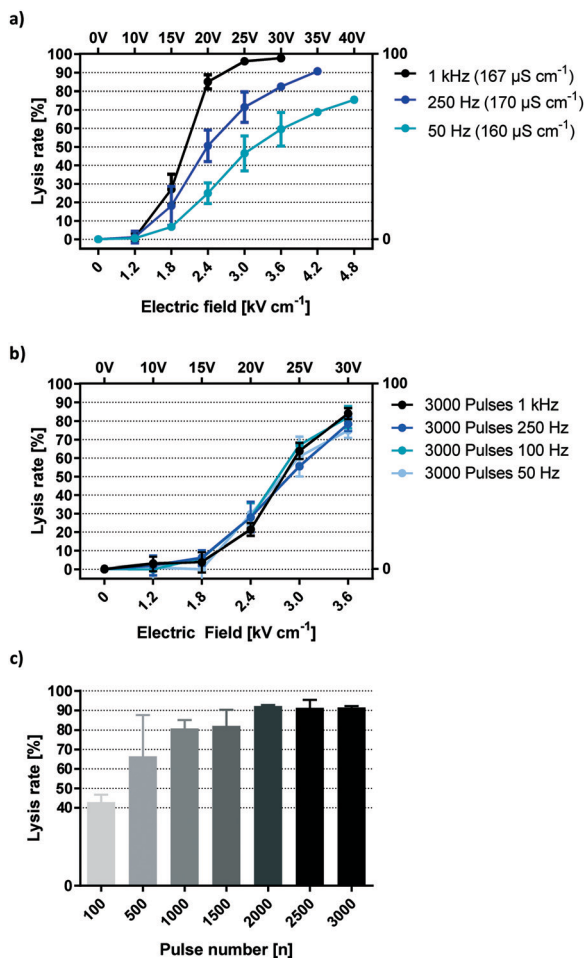


Fig. 4 Frequency dependency of electric field mediated lysis with capacitive coupling. a) Frequency dependency of HEK-293 lysis with equal field exposure time. b) HEK-293 lysis at different frequencies, exposure time adjusted to 3000 pulses. c) Lysis efficiency of different pulse numbers at 1 kHz. (a–c) $\sigma = 160\text{--}170\ \mu\text{S cm}^{-1}$, $n = 3$.

adjusted so that the number of pulses is equal for all frequencies (Fig. 4b). Typical for this conductivity, onset of cell disruption was seen at $1.8\ \text{kV cm}^{-1}$ while a plateau was reached by $3.6\ \text{kV cm}^{-1}$. With equal pulse numbers, lysis curves are aligned at all field strengths irrespective of frequency. This shows that coupled-field lysis dynamics are in fact frequency independent for square wave pulses when correcting exposure time for the number of pulses.

Additional insights are gained by applying this information back to Fig. 4a and multiplying the indicated frequency with the total exposure time of 6 seconds. This reveals lysis information for 300 (50 Hz), 1500 (250 Hz) and 6000 (1 kHz) square wave pulses.

Notice that maximum lysis was approached for 6000 pulses at 25 V and 30 V but not for lower pulse numbers. This suggests a threshold number of 1500 to 6000 pulses required to yield a maximum electric field effect at the given voltage.

To identify the threshold pulse quantity for efficient lysis, a broader range of pulses were investigated (Fig. 4c). Field

strength was set to $3.6\ \text{kV cm}^{-1}$ and frequency to 1 kHz. As a result, lysis efficiency increased steadily with pulse numbers up to 2000, reaching a plateau of maximum efficiency with around 90% lysis and minimal SD. We postulate that such a pulse threshold exists for any field strength high enough to cause cell lysis. This section demonstrates that HEK-293 lysis was independent of square wave frequencies between 50 Hz and 1 kHz but increases with the number of applied AC square wave pulses. This means that the lysis effect corresponds to a change in voltage (dU/dt) rather than the absolute voltage (U). In practice, this parameter is best monitored by observing the capacitive charging current which is always proportional to (dU/dt). As such, we can derive the relative electric field effect of a capacitively coupled setup simply by looking at its current plot.

If the number of times that the field direction is inverted is the only factor governing cell lysis at a specific field strength, then the time that passes between one such charge alternation and the next is also negligible in the given frequency range. In other words, it makes no difference whether the voltage is sustained for 10 ms (half-period for 50 Hz) or 0.5 ms (1 kHz) between inversions (Fig. 4b). This implies that the membrane effect that is elicited by our setup is cumulative and has a decay time longer than 10 ms.

Efficient propidium iodide delivery with limited cell death can be achieved with high and low energy pulses

Membrane permeabilization occurs prior to cell lysis.²⁴ With knowledge of the lysis threshold of HEK-293 cells, it is possible to approximate at which setting membrane permeabilization takes place with minimal cell lysis. Fig. 5a shows lysis and PI-permeabilization of HEK-293 cells when exposed to a decreasing number of high-voltage square wave pulses. 50 pulses of 40 V lead to lysis of 48.5% of cells while PI was taken up by 78.8% of the remaining viable cells. Decreasing the number of pulses further resulted in higher viability while the fraction of live cells permeable to PI remained similar. Upon exposure to 5 square wave pulses of 40 V, 5.6% of HEK-293 cells were lysed by the electric field while 82.8% were viable and PI-positive. Fig. 5b shows further optimization of PI-delivery by changing the applied voltage. Cells were subjected to 5 square wave pulses at 1 kHz repetition rate. Viability was virtually unaltered by potentials lower than 45 V. HEK-293 cell viability was decreased by 1.8% upon application of five 25 V pulses while five 40 V pulses decreased viability by 2.5%. Because these minor viability changes do not correlate with the field increase, the recorded cell death was most likely caused by the working protocol rather than any specific field effect. Electrical cell lysis can be assumed to take place when further increasing the field to 45 V, resulting in a more significant viability reduction of 13.7%.

Fig. 5b shows a correlation between field strength and the fraction of PI-permeable cells, yielding 22.4%, 66.7%, 82.3%, 80.5% and 81.1% for 25 V, 30 V, 35 V, 40 V and 45 V,



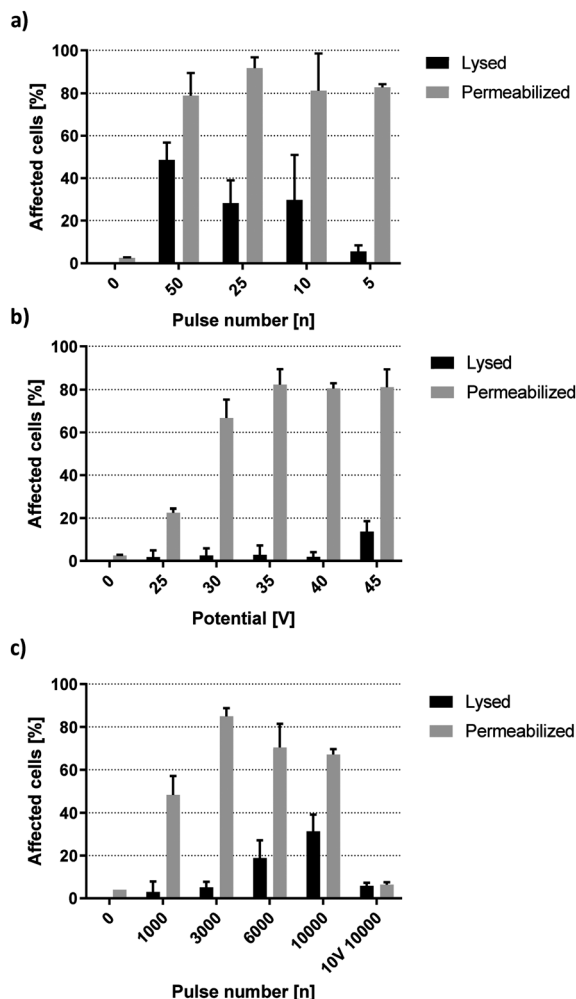


Fig. 5 Propidium iodide delivery with capacitive coupled electric fields. HEK-293 cell lysis and permeabilization after exposure to a) decreasing pulse number of 40 V square waves, b) 5 square wave pulses of increasing voltage and c) an increasing number of 15 V square wave pulses. Permeabilized refers to the percentage of remaining live cells. $f = 1$ kHz, $\sigma = 160 \mu\text{S cm}^{-1}$, $n = 3$.

respectively. The sharp increase between 25 V and 35 V as well as the following plateau of maximum permeabilization between 35 V and 45 V was reminiscent of dynamics observed from lysis experiments in the previous section. This implies the existence of distinct but separate energy thresholds for complete permeabilization or lysis of HEK-293 cells. Looking back at Fig. 4a reveals that onset of lysis was pulse number dependent from 15 V upward. Fig. 5c further shows that PI-permeabilization was strongly correlated with pulse number at 15 V. 1000 square wave pulses yielded 48.4% PI-positive viable HEK-293 cells, increasing up to 85.0% at 3000 pulses with minimal loss of viability. A further increase in pulse number did not improve PI delivery but rather increased the rate of electrical cell lysis. Interestingly, the permeabilization of remaining live cells did not remain at a plateau of ~80% as was the case for high voltage pulses but decreased steadily (Fig. 5c). However, the total amount of HEK-293 cells affected by the field remained relatively stable, with the sum of lysed

or permeabilized cells being 85.8%, 76.0% and 77.4% for 3000, 6000 and 10 000 pulses, respectively (not shown). As such, these numbers do not account for a difference in field penetration at different voltages but rather indicate the cumulative biological effect of this specific field magnitude. Additionally, cells exposed to 10 000 pulses of 10 V were not affected by the electric field. This indicates the existence of a minimum threshold for HEK-293 specific membrane permeabilization between 10 V and 15 V corresponding to a theoretical field strength between 1.2 and 1.8 kV cm^{-1} .

Mammalian cell transfection is feasible with high- k passivated electrodes

Given the efficiency of small molecule transfer observed in the previous section, we proceeded to assess if these settings may be applied towards gene delivery. According to Fig. 5b, high-energy pulses yield the largest window of opportunity for high-efficiency permeabilization. Consequently, square wave pulses of 40 V were chosen for initial transfection experiments. Fig. 6c shows HEK-293 cells expressing TurboRFP 48 hours after electro-transfection with pTurboRFP-N plasmid. The application of 10 square wave pulses resulted in average transfection efficiencies of 4.6%. This seems surprisingly low, given that the field thresholds required for PI and plasmid delivery are known to be similar.³² However, it was shown that efficient transfection by electric fields is improved by a unidirectional electrophoretic component that facilitates DNA movement.^{7,32,33} Remembering the insights about capacitively coupled pulse dynamics revealed by their frequency independency (Fig. 4a and b), we find that each period of a square wave has two equal and opposite peaks which fail to provide net DNA movement (Fig. 6a). To achieve a unidirectional, electrophoretic force component with capacitive coupling, the slopes of the voltage plot need to be

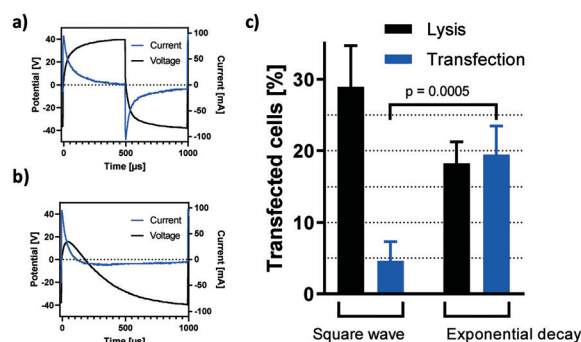


Fig. 6 Transfection by capacitive coupling. Pulse characteristics of EPB subjected to a) square wave and b) exponential decay pulses of 40 V at 1 kHz. $\sigma = 160 \mu\text{S cm}^{-1}$ c) capacitively coupled, electric field mediated transfection of HEK-293 cells with pTurboRFP-N plasmid. Bars show the percentage of cells lysed (black bars, $n = 3$) or expressing RFP 48 hours after field exposure as detected and quantified by fluorescence microscopy (blue bars). $f = 1$ kHz, $\sigma = 161 \mu\text{S cm}^{-1}$, square wave: $n = 3$, exponential decay: $n = 8$.



asymmetric. One example is the use of an exponential decay function in which $\Delta U/dt$ is maximised in one direction and sufficiently reduced in the other (Fig. 6b). In this case, the applied voltage rises instantly and drops exponentially from +40 V to -40 V over the course of one 20 ms period. As revealed by the current plot, a significant electric field effect occurs exceedingly in the positive direction. Fig. 6c shows that such exponential decay pulses result in a significant increase of plasmid delivery events to 19.5% of cells. This confirms the impact of an electrophoretic component on the complex process of DNA delivery and shows how capacitive coupling can be utilized for gene transfer. As can be expected from the corresponding current plots (Fig. 6a and b), the impact on cell lysis is reduced by the exponential decay pulse (Fig. 6c).

We propose that a modified high-*k* passivation layer with increased capacity allows for higher net movement of plasmid DNA per pulse application and thereby increases the rate of transfection.

Conclusion

The introduction of electrode passivation with high-*k* material for capacitive coupling of electric fields drastically increases the consistency of electroporation events, offers superior control of relevant variables and thereby allows for the detailed assessment of parameter changes. This was achieved by the reduction of faradaic current across the working solution at biologically relevant voltages. The implementation of titanium dioxide coated electrodes in a stationary design demonstrates the versatility and applicability of this concept in microfluidic devices. Both the passivation- and assembly procedures are simple, cost efficient and yield prototypes that have a consistent biological outcome. The necessity of electrode passivation in this microfluidic design was showcased by experiments with unpassivated electrodes, which do not allow for an indicative readout of the parameter changes. Experiments with HEK-293 cells reveal clear and distinct dependencies between experimental parameters and biological outcome in terms of both lysis and permeabilization. Most notably, manual prototype assembly has less impact on cell lysis than any other tested variable.

In summary, this system offers the unique opportunity to study the impact of alternating electrical fields on biological suspensions by excluding the superimposing effects of electrochemistry. We demonstrate its applicability towards cell lysis, cargo transfer and transfection. The efficiency of transfection is expected to increase with further optimization of the presented platform in terms of current and passivation layer characteristics.

Author contributions

TW, JRP, EKE and KJW are responsible for conceptualization of the idea. TW conducted data curation and formal analysis.

KJW is responsible for funding acquisition. TW is responsible for investigation and specifically performed experiments and data acquisition. TW, EKE and KJW developed the methodology. EKE and KJW are responsible for administration, resources and supervision. TW is responsible for validation. TW, JRP, EKE and KJW are responsible for visualization, preparation, creation and presentation of the published work. TW wrote the original draft. TW, JRP, EKE and KJW are responsible for review and editing. All authors have read and approved the manuscript.

Conflicts of interest

We declare that the authors Terje Wimberger, Johannes R. Peham and Klemens J. Wassermann have filed a patent application (date: 12.12.2018; application number: EP18211969.3) on behalf of the Austrian Institute of Technology which includes the following aspects of the manuscript: the passivation strategy, stationary prototype design and their application towards cell lysis, permeabilization and transfection. Eva-Kathrin Ehmoser has no conflicts of interest to declare.

Acknowledgements

The authors would like to acknowledge the Austrian Institute of Technology GmbH as the source of funding for this project. We wish to thank Seta Küpcü from the Department of Nanobiotechnology at BOKU University for considerations that went into choosing HEK-293 cells as a model for this article. Special thanks go to Christina Bliem for her assistance in the graphical design of the prototype in Scheme 1.

References

- 1 J. C. Weaver, *IEEE Trans. Plasma Sci.*, 2000, **28**, 24–33.
- 2 R. S. Son, K. C. Smith, T. R. Gowrishankar, P. T. Vernier and J. C. Weaver, *J. Membr. Biol.*, 2014, **247**, 1209–1228.
- 3 J. C. Weaver, K. C. Smith, A. T. Esser, R. S. Son and T. R. Gowrishankar, *Bioelectrochemistry*, 2012, **87**, 236–243.
- 4 V. Dimitrov, S. Kakorin and E. Neumann, *Phys. Chem. Chem. Phys.*, 2013, **15**, 6303–6322.
- 5 H. M. Eppich, R. Foxall, K. Gaynor, D. Dombkowski, N. Miura, T. Cheng, S. Silva-Arrieta, R. H. Evans, J. A. Mangano, F. I. Pfeffer and D. T. Scadden, *Nat. Biotechnol.*, 2000, **18**, 882–887.
- 6 L. Lambricht, A. Lopes, S. Kos, G. Sersa, V. Pr  at, G. Vandermeulen and Expert Opin, *Drug Delivery*, 2016, **13**, 295–310.
- 7 C. Rosazza, S. H. Meglic, A. Zumbusch, M.-P. Rols and D. Miklavcic, *Curr. Gene Ther.*, 2016, **16**, 98–129.
- 8 J. A. Kim, K. Cho, M. S. Shin, W. G. Lee, N. Jung, C. Chung and J. K. Chang, *Biosens. Bioelectron.*, 2008, **23**, 1353–1360.
- 9 J. A. Kim, K. Cho, Y. S. Shin, N. Jung, C. Chung and J. K. Chang, *Biosens. Bioelectron.*, 2007, **22**, 3273–3277.
- 10 P. Turjanski, N. Olaiz, F. Maglietti, S. Michinski, C. Suarez, F. V. Molina and G. Marshall, *PLoS One*, 2011, **6**, e17303.



- 11 A. Meir and B. Rubinsky, *RSC Adv.*, 2014, 4, 54603–54613.
- 12 A. Ainla, S. Xu, N. Sanchez, G. D. M. Jeffries and A. Jesorka, *Lab Chip*, 2012, 12, 4605–4609.
- 13 N. Jokilaakso, E. Salm, A. Chen, L. Millet, C. D. Guevara, B. Dorvel, B. Reddy, A. E. Karlstrom, Y. Chen, H. Ji, R. Sooryakumar and R. Bashir, *Lab Chip*, 2013, 13, 336–339.
- 14 D. Zhao, D. Huang, Y. Li, M. Wu, W. Zhong, Q. Cheng, X. Wang, Y. Wu, X. Zhou, Z. Wei, Z. Li and Z. Liang, *Sci. Rep.*, 2016, 6, 18469.
- 15 L. Chopinet and M.-P. Rols, *Bioelectrochemistry*, 2015, 103, 2–6.
- 16 H. Lu, M. A. Schmidt and K. F. Jensen, *Lab Chip*, 2005, 5, 23–29.
- 17 L. Nan, Z. Jiang and X. Wei, *Lab Chip*, 2014, 14, 1060–1073.
- 18 T. Geng and C. Lu, *Lab Chip*, 2013, 13, 3803–3821.
- 19 A. Rolong, E. M. Schmelz and R. V. Davalos, *Integr. Biol.*, 2017, 9, 979–987.
- 20 T. S. Santra, C.-W. Chen, H.-Y. Chang and F.-G. Tseng, *RSC Adv.*, 2016, 6, 10979–10986.
- 21 K. J. Wassermann, S. Barth, F. Keplinger, C. Noehammer and J. R. Peham, *ACS Appl. Mater. Interfaces*, 2016, 8, 21228–21235.
- 22 H. Shafiee, J. L. Caldwell, M. B. Sano and R. V. Davalos, *Biomed. Microdevices*, 2009, 11, 997–1006.
- 23 M. B. Sano, J. L. Caldwell and R. V. Davalos, *Biosens. Bioelectron.*, 2011, 30, 13–20.
- 24 T. Kotnik, A. Macek-Lebar, D. Miklavcic and L. M. Mir, *BioTechniques*, 2000, 28, 921–926.
- 25 M. Bonakdar, P. M. Graybill and R. V. Davalos, *RSC Adv.*, 2017, 7, 42811–42818.
- 26 S. R. A. Kratz, C. Eilenberger, P. Schuller, B. Bachmann, S. Spitz, P. Ertl and M. Rothbauer, *Sci. Rep.*, 2019, 9, 9287.
- 27 J. Schindelin, I. Arganda-Carreras, E. Frise, V. Kaynig, M. Longair, T. Pietzsch, S. Preibisch, C. Rueden, S. Saalfeld, B. Schmid, J.-Y. Tinevez, D. J. White, V. Hartenstein, K. Eliceiri, P. Tomancak and A. Cardona, *Nat. Methods*, 2012, 9, 676–682.
- 28 S. Li, *Cold Spring Harbor Prot.*, 2006, <http://cshprotocols.cshlp.org/content/2006/1/pdb.prot4449.abstract>.
- 29 G. Pucihar, T. Kotnik, M. Kanduser and D. Miklavcic, *Bioelectrochemistry*, 2001, 54, 107–115.
- 30 C. S. Djuzenova, U. Zimmermann, H. Frank, V. L. Sukhorukov, E. Richter and G. Fuhr, *Biochim. Biophys. Acta, Biomembr.*, 1996, 1284, 143–152.
- 31 M.-P. Rols and J. Teissié, *Biophys. J.*, 1998, 75, 1415–1423.
- 32 M. Pavlin and M. Kandušer, *Sci. Rep.*, 2015, 5, 9132.
- 33 M. M. Sadik, M. Yu, M. Zheng, J. D. Zahn, J. W. Shan, D. I. Shreiber and H. Lin, *Biophys. J.*, 2014, 106, 801–812.



2.2 Capacitive coupling increases the accuracy of cell-specific tumour disruption by electric fields

Authors

Terje Wimberger,^{ab} Verena K. Köhler,^{ac} Eva K. Ehmoser,^b Klemens J. Wassermann^a

Affiliations

^a Austrian Institute of Technology GmbH, Department for Health & Bioresources, Vienna, Austria.
E-mail: Terje.wimberger@ait.ac.at, Klemens.wassermann@ait.ac.at

^b BOKU - University of Natural Resources and Life Sciences, Department for Nanobiotechnology, Vienna, Austria

^c BOKU - University of Natural Resources and Life Sciences, Department for Biotechnology, Vienna, Austria

Author contributions

Terje Wimberger: Conceptualization, Methodology, Investigation, Writing - original draft, Writing - review & editing, Visualization. **Verena K. Köhler:** Methodology, Investigation, Visualization. **Eva K. Ehmoser:** Conceptualization, Resources, Writing - review & editing, Supervision. **Klemens J. Wassermann:** Conceptualization, Methodology, Investigation, Resources, Writing - review & editing, Supervision, Project administration, Funding acquisition.

Author comment

Earlier works on differential cell lysis by capacitive coupling utilized the absence of electrochemistry in a whole-blood sepsis model. The isolation of bacteria spiked in whole-blood was possible due to their much higher resistance to electric-field mediated lysis. While this difference in field susceptibility applies to all electroporation platforms, based on the smaller size and higher membrane capacitance of bacteria, the necessity of passivation is grounded in the incredible signal-noise ratio of the model. With a ml of blood containing around 5×10^9 mammalian cells compared to about 10 bacteria during acute systemic sepsis, unspecific chemical lysis of bacterial cells had to be entirely abolished. Subsequent experiments featuring different mammalian cell types revealed surprising differences in the lysis dynamics of specific lineages. The most significant observation was the incredible resistance to field-mediated lysis displayed by human leukocytes when capacitive coupling was employed. Contrary to conventional electroporation, erythrocyte lysis takes place at much lower field magnitudes. This enables electric fields to be used for specific enrichment of leukocytes from biological isolates, a feature unique to our platform since the order of field susceptibility is reversed when using ohmic coupling. Another surprising discovery was made in the lysis dynamics of leukemia and CTC models that are characterized by an even higher susceptibility to electric field strength than red blood cells. While the causes for discrepancies between capacitive and ohmic lysis dynamics remain unaccounted for, the reasoning in the manuscript is complemented by a thorough assessment of relevant variables in the discussion of this thesis (section 3.2).



Capacitive coupling increases the accuracy of cell-specific tumour disruption by electric fields

Terje Wimberger^{a,b,*}, Verena K. Köhler^{a,c}, Eva K. Ehmoser^b, Klemens J. Wassermann^{a,*}

^aAIT – Austrian Institute of Technology GmbH, Department of Health & Bioresources, Vienna 1210, Austria

^bBOKU – University of Natural Resources and Life Sciences, Department of Nanobiotechnology, Vienna 1190, Austria

^cBOKU – University of Natural Resources and Life Sciences, Department of Biotechnology, Vienna 1190, Austria

ARTICLE INFO

Article history:

Received 25 October 2019

Received in revised form 24 February 2020

Accepted 24 February 2020

Available online 29 February 2020

Keywords:

Capacitive coupling

Cell lysis

Electroporation

Microfluidics

Tumour ablation

ABSTRACT

Irreversible electroporation holds great potential for cell-specific lysis due to the size-dependent susceptibility of cells to externally imposed electric fields. Previous attempts at selective cell lysis lead to significant overlap between affected populations and struggle with inconsistent biological outcome. We propose that charge transfer at the electrode-liquid interface is responsible by inducing multifactorial effects originating from both the electric field and electrochemical reactions. A promising remedy is the coating of electrodes with a high- k dielectric layer. The resulting capacitive coupling restores the selective potential of electric field mediated lysis in a microfluidic setup. Initial experiments show the consistent depletion of erythrocytes from whole blood while leaving leukocytes intact. The same is true for the reproducible and selective depletion of Jurkat and MCF-7 cells in a mixture with leukocytes. Unexpectedly, the observed order of lysis cannot be correlated with cell size. This implies that the cellular response to capacitive coupling features a selective characteristic that is different from conventional lysis configurations.

© 2020 Published by Elsevier B.V.

1. Introduction

Biological membranes exposed to an electric field of sufficient magnitude undergo electroporation, corresponding to an increase in permeability of the lipid bilayer [1,2]. If the field is further increased and the transmembrane potential reaches a critical threshold, the effect becomes irreversible and leads to cell lysis [3,4]. The known factors governing changes in the local transmembrane potential are described by

$$\psi_{m_{\text{initial}}} = \frac{3}{2}ER \cos(\theta) (1 - e^{-t/\tau_m}) \quad (1)$$

where E is the externally applied electric field, R is the cell radius, θ being the angle between the electric field direction and the point on the membrane affected by the field, t being the field exposure time and τ_m being the membrane charging time [5,6]. Since the change in transmembrane potential is co-determined by cell size, a window of

opportunity for selective cell lysis is implied and has been exploited for selective lysis on previous occasions [7,8].

To our knowledge, three prior studies have attempted the electric field-mediated lysis of malignant cells from blood. The first study featured in *Nature Biotechnology* was confined to a batch configuration [8]. Acute Megakaryocytic Leukemia (CMK) cells were spiked with peripheral blood mononuclear cells and showed a higher susceptibility to electric fields. At settings that deplete > 98% of CMK cells, monocyte viability is reduced below 20%. Shortcomings in the electrical setup result in 67% confidence intervals for 7 repetitions and the need for a water-cooling system to counter significant joule heating. The second study was featured in *Blood* and shows the efficient depletion of multiple myeloma cell lines from blood [9]. While it was shown that stem cell function of the surviving population was preserved, less than 1% of monocytes and 10% of lymphocytes survived the treatment. In the third study published in *Lab on a Chip*, 98% of M109 circulating tumour cells are eliminated by field magnitudes at which > 50% of white blood cells remain non-viable [10].

The biggest obstacle for using electric fields in a cell-specific manner is the multifactorial nature of the effect. While the field effect might be considered specific, it is inevitably accompanied by a number of non-specific side effects caused by electrochemical events along the electrode-suspension interface [11]. These include

* Corresponding authors at: AIT – Austrian Institute of Technology GmbH, Department of Health & Bioresources, Giefinggasse 4, Vienna 1210, Austria (T. Wimberger).

E-mail addresses: terje.wimberger@ait.ac.at (T. Wimberger), klemens.wassermann@ait.ac.at (K.J. Wassermann).

pH- and temperature changes as well as ionic radicals and gas formation, which in turn negatively affect reproducibility, cellular integrity and electrode lifetime [12,13].

Strategies to minimize the impact of electrochemistry have included spatial separation of electrodes [12]. A downside of large electrode distance is the high voltage required to reach a sufficient local electric field. Nanosecond pulse electroporation represents another method of tackling the issue of electrochemistry, but similarly requires high voltages and specialized equipment [14]. Microfluidic approaches to reduce the adverse effects of electrolysis encounter a different set of obstacles; complex geometries lead to loss of field uniformity and highly miniaturized systems are accompanied by cell deformation and limited throughput [15,16]. In summary, there is no consensus on the method of choice for applying uniform electric field effects to a sufficient number and fraction of cells.

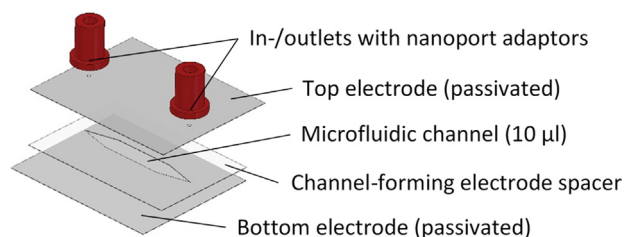
Since all the discussed side effects are detrimental to a fraction of any given cell population, discussing the issue of cell specific lysis is somewhat misleading because the real challenge is posed by specifically keeping a certain cell population intact. In a previous publication, we presented an alternative approach to deal with unspecific side effects posed by electrochemistry; by coating electrodes with a high- k passivation layer, we were able to deliver sufficient electric fields to a cell suspension while significantly reducing electrochemical reactions along the interface [17]. This is a result of capacitive coupling, which also has a history of use in contactless dielectrophoresis. There, it has successfully resolved issues associated with electrode fouling during continuous low-energy field application at high frequencies [18,19].

The theoretical possibility of size discrimination was successfully put into practice for large differences in size, such as between bacteria and mammalian cells [20]. Subsequent work revealed that our device can specifically target cell populations of similar size. Sticking to our established model of whole blood (WB) lysis, we present the selective, field-mediated lysis of erythrocytes as a novel method for leukocyte isolation and proceed to demonstrate the selective elimination of malignant cells from isolated leukocytes.

2. Materials and methods

2.1. Electrode passivation and prototype assembly

Details on optimization of the passivation procedure and design considerations are provided in a previous publication [20]. Briefly, commercial titanium foils (grade 2, cpTi, 99.2% purity, 110 μm thick) were cut and 0.8 mm holes drilled to form in- and outlet ports. Foils were cleaned in ultrasonic bath with a series of acetone, ultrapure water and isopropanol for 20 min each. This was followed by thermal oxidation in a muffle furnace (L 9/11 P330, Schaefer & Lehmann, Germany) for 3 h at 650 $^{\circ}\text{C}$ with 2 h rise-time and passive cooling to room temperature (RT). Microfluidic cell lysis units were assembled by cutting the flow chamber geometry (Schematic 1) into double-sided 81.3 μm thick adhesive tape (Arcare 90445, Adhesive Research, Ireland), sandwiched by two pieces of passivated titanium foil. The adhesive features continuous thickness, bio-compatibility [21] and yields a channel volume of 10 μl . Adaptors to the flow system (NanoPort Std 6-32 Coned 1/32, IDEX, USA) were fixed to in- and outlets. Circuit closure was ensured by removal of outer oxide layer from the bottom sides of both electrodes using diamond files until the resistance dropped below 1 Ω . Every new prototype was assessed in term of fluidics and electrical performance by application of standard pulses when filled with phosphate buffered saline (PBS).



Schematic 1. Geometric design of the electric cell lysis unit. The fluidic channel is formed by double-sided adhesive tape. Dimensions in length \times width \times height; Electrodes: 37.5 \times 25 \times 0.1 mm. Fluidic channel: 30 \times 5 \times 0.081 mm whereby 5 mm refers to the maximum width.

2.2. Preparation of working solutions

Preparation of the electroporation buffer (EPB) was performed by incremental addition of PBS to autoclaved 250 mM sucrose solution until conductivity reached 100 $\mu\text{S}/\text{cm}$. WB samples were directly diluted in 250 mM sucrose without conductivity manipulation. Conductivity was measured using a conductivity meter (B-771 LAQUATwin, HORIBA Advanced Techno, Japan). WB was collected from healthy volunteers using K3-EDTA collection tubes (Vacuette, Greiner Bio One, Austria), immediately stored at 4 $^{\circ}\text{C}$ and kept for a maximum of 3 days. Erythrocyte lysis buffer (ELB) containing 155 mM NH_4Cl , 10 mM KHCO_3 and 0.1 mM EDTA was prepared, sterilized by filtration (0.22 μm PVDF filter) and stored at 4 $^{\circ}\text{C}$ until use.

2.3. Cell culture

Jurkat T lymphocytes as a model for human acute T lymphocyte leukaemia (Clone E61, ATCC[®]TIB152[™]) were cultivated at 37 $^{\circ}\text{C}$ and 5% CO_2 in RPMI (Thermo Fisher, 21875091) supplemented with 10% FBS (Thermo Fisher, 10500) and 1% Pen/Strep Antimycotic-Antimycotic (Thermo Fisher, 15240). Jurkat T lymphocyte suspension cultures were passaged by transferring a fraction of the suspension to a 15 ml tube, centrifuging for 5 min at 400 rcf (RT, Eppendorf 5430; Rotor: F-35-6-30), re-suspension in fresh medium and transfer to cultivation flask.

Michigan Cancer Foundation-7 breast cancer cell line (MCF-7) as a model for circulating tumour cells (Public Health England, 86012803, Lot No. 141018) were cultivated at 37 $^{\circ}\text{C}$ and 5% CO_2 in MEM (Thermo Fisher, 21875091) supplemented with 10% FBS (Thermo Fisher, 10500), 2% L-Glutamine (Thermo Fisher, 25030081), 1% non-essential amino acids (Thermo Fisher, 11140050) and 1% Pen/Strep Antimycotic-Antimycotic (Thermo Fisher, 15240). MCF-7 were passaged by washing with PBS (1x from stock: Thermo Fisher, 70011044) followed by trypsinization (0.25%, Thermo Fisher, 25200) for 5 min at 37 $^{\circ}\text{C}$. Any sterile protocols were processed in biological safety cabinets (Herasafe KS, Class II, Thermo Fisher, 51022488).

2.4. Leukocyte isolation

10 ml ELB was mixed with 1 ml of WB, incubated 10 min at RT and inverted repeatedly. The suspension was centrifuged at 500 rcf for 10 min at RT (Eppendorf 5430; Rotor: F-35-6-30). These steps were repeated until a white cell pellet was obtained (indicating erythrocyte depletion). After washing twice with sucrose-PBS solution set to 100 $\mu\text{S}/\text{cm}$, cells were counted, and concentration was adjusted to 5 \times 10⁵ cells/ml. Lysis was assessed by staining with Hoechst 33342 (Ref.: B2261, Sigma-Aldrich Co. LLC.). Preparations exceeding 20% lysis in the 0 V control were discarded.

2.5. Preparation of Jurkat T lymphocytes and MCF-7 culture cells

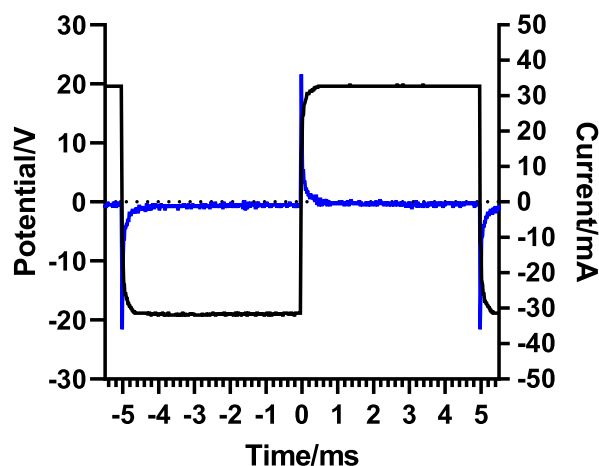
Jurkat T lymphocyte suspension was centrifuged at 400 rcf for 5 min and excess medium discarded. Cells were re-suspended in 5 ml EPB (100 μ S/cm). This step was repeated three times. During the last centrifugation step, an aliquot of cells was counted and re-suspended in the amount of EPB needed for a final cell concentration of 5×10^5 cells/ml and the suspension conductivity recorded. Adherent MCF-7 cells were washed with PBS, trypsinized for 5 min at 37 °C and re-suspended in culture medium. Further preparation steps were performed analogous to Jurkat preparation.

2.6. Preparation of spike-in suspensions

For the WB-leukocyte spike-in experiments, leukocytes prepared as in Section 2.4 were equilibrated in EPB with a conductivity of 210 μ S/cm and a final concentration of 10^6 cells/ml. WB was diluted 1:500 in EPB (210 μ S/cm) and counted. Further EPB was added to adjust cell concentration to 10^6 cells/ml. Both suspensions were mixed 1:1 prior to field exposure. For the Jurkat T lymphocyte-spiked leukocyte suspension, both populations were prepared as described in Sections 2.4 and 2.5, but with an increased concentration of 10^6 cells/ml, respectively. Jurkat T lymphocytes in EPB were stained with 10 nM Calcein-AM solution (Thermo Fischer, C3100MP) for 60 min at 37 °C to allow for population tracking in flow cytometry. An aliquot of unstained cells was set aside for flow cytometry negative controls. Prior to pulse application, stained Jurkat T lymphocytes were mixed 1:1 with leukocytes for final concentrations of 5×10^5 cells/ml each. For the MCF-7-spiked leukocyte suspension, both populations were prepared as described in Sections 2.4 and 2.5 with cell counts increased to 10^6 cells/ml. MCF-7 cells in EPB were stained with a 1:20 dilution of FITC Anti-human CD326 (Biolegend, Cat.no. 324204) for 30 min at 4 °C to allow for population tracking in flow cytometry. An aliquot of unstained cells was set aside for flow cytometry negative controls. Prior to pulse application, stained MCF-7 are mixed 1:1 with leukocytes for final concentrations of 5×10^5 cells/ml each. Live-dead discrimination of the MCF-7 population was assessed by Hoechst 33342 staining (1 μ g/ml) prior to data acquisition.

2.7. Electric field application

1 ml of respective cell suspension was transferred to a 1 ml syringe (Omnifix-F, Braun, Germany) and injected to the electric cell lysis unit (ECLU) by a syringe pump (Fusion 200 Touch, KR Analytical Ltd, United Kingdom) set to a flow rate of 100 μ l/min. To discriminate between parameters, at least five ECLU chamber volumes – a total of 50 μ l – were passed through the device after any parameter change and before collecting an aliquot for further analysis. Respective voltages refer to square waves applied by a function generator (DG4102, Rigol) connected to a voltage amplifier (Falco WMA-300, Falco Systems, Netherlands). Voltage and current (via a 2 Ω resistor) were monitored by an oscilloscope (DS1104B, Rigol). Given the channel volume of 10 μ l, a flow rate of 100 μ l/min means that cells are exposed to the indicated field parameters for 6 s. A frequency of 100 Hz results in 600 square wave periods. Notably, this does not imply that cells are subjected to 6 s of sustained electric field (Schematic 2). As outlined in a previous publication, the field effect relevant for cell manipulation is of transient nature, only applies during capacitive charging and is therefore proportional to the initial and short (μ s-range) charging current [17]. All indicated voltages refer to the maximum potential at the electrodes after capacitive charging is completed (Schematic 2). These voltages are proportional, but not equal to the effective



Schematic 2. Voltage (black) and current (blue) characteristics of a passivated electric cell lysis unit when 20 V are applied to a 100 μ S/cm solution of electroporation buffer at 100 Hz. (For interpretation of the references to colour in this figure legend, the reader is referred to the web version of this article.)

electric field inside the electroporation medium. This means that any voltage increase in experiments refers to a relative increase in electric field and that the voltage used for single experiments is only relevant in the context of previous experiments covering a similar voltage range under the same conditions. An accurate measure of field strength cannot be readily provided for capacitive coupling with a liquid interface. Simulation studies on conceptually similar designs reveal dependencies on conductivity, temperature, thickness of the passivation layer and dielectric constant [13]. The only experimental readout we are aware of was based on an optical measurement of the Kerr effect [22]. This was only possible with significant restrictions to the design which are incompatible with our platform.

2.8. Data acquisition and analysis

Temperature increase was measured by directly attaching a wireless, infrared thermometer (Texas Instruments SensorTag CC2541) to the bottom of the prototype with the sensor positioned below the fluid channel. Temperature change of EPB upon application of 30 V square waves at 100 Hz was recorded in 15 s intervals.

Lysis rate was assessed by transferring a 10 μ l aliquot of ECLU-treated cell suspensions to a haemocytometer (Thoma, Optik Labor) and imaging with a digital camera (Prosilica GT, Allied Vision) mounted on an inverted microscope (CKX41 Fluo V2, Olympus). Bright-field images were recorded for total cell count. For leukocytes, Jurkat T lymphocytes and MCF-7 cells, 1 μ g/ml Hoechst 33342 viability dye was added to discriminate dead cells. For assessing the lysis behaviour of leukocytes in WB-leukocyte spike-in experiments, 1 μ g/ml of membrane impermeable Propidium Iodide (PI) was added after field exposure and prior to imaging. Flow cytometry data acquisition of (Jurkat T lymphocyte and MCF-7) spike-in experiments was performed with BD FACSCanto II. Forward scatter (FSC) and side scatter (SSC) thresholds were set to eliminate cell debris from the final readout. 10 000 events were recorded for each parameter. Ca-AM and CD326-FITC parameters were recorded in the FITC channel, Hoechst 33342 staining was recorded in the Pacific Blue channel. Data was gated in Flowing Software 2.5.121 and statistical evaluation and data visualization carried out with GraphPad Prism 7. Where applicable, standard deviation (SD) refers to SD of all replicates and n refers to technical replicates. Flow cytometry data was composed from biological replicates as indicated.

3. Results and discussion

3.1. High- k passivation limits joule heating

A persisting issue in microfluidic, electric field applications is the limited throughput of batch configurations and the complexity of circumventing negative side effects of electrochemistry in flow-through setups [16], the consequences of which have been outlined in the introduction. Our previous investigations on this topic have examined the rate of electrochemistry along the electrode interface via cyclic voltammetry and concluded that passivation significantly increases the charge transfer resistance at the liquid-electrode interface [17]. Fig. 1 complements this information by revealing the temperature stability of the flow-through design (Schematic 1) with high- k passivated electrodes for 10 min of continuously applied square wave pulses (30 V at 100 Hz). Without passivation, temperature increases by 16.3 °K when processing 1 ml of sample. A 10 °K increase is reached within 3 min of pulse application. The highest sensor noise recorded was $\Delta 0.16$ °K. With high- k passivation, a maximum temperature increase of 0.67 °K is observed after 540 s of field application. This value accounts for the processing of 1 ml of sample at 100 μ l/min at a voltage sufficient for all lysis applications in the following experiments. In the passivated device, current flow is restricted to capacitive charging and returns to zero when the maximum potential is reached (μ s-range, Schematic 2). This means that current flow and therefore input power is significantly reduced when compared to the configuration with ohmic coupling. Fig. 1 demonstrates that temperature effects do not have to be considered or remedied during sustained pulse application with passivated flow-through prototypes.

3.2. Electric field mediated erythrocyte lysis is conductivity dependent

This section shows erythrocyte lysis at varying field strength and buffer conductivity as a result of WB dilution with 250 mM sucrose. Previous examinations of the correlation between buffer conductivity and electric field mediated lysis have resulted in contradicting reports; Pucihar *et al.* reported reduced field effects on DC3F Chinese hamster fibroblasts when reducing medium conductivity in the range of 0.01–16 mS/cm [23]. Such negative correlations are further found by Ivorra *et al.* [24] and Rols and Teissie [3]. Contradicting, Djuzenova *et al.* found that reducing conductivity between 0.8 and 14 mS/cm increased electroporation of murine myeloma cell line Sp2/0-Ag14 [25]. Such a positive correlation was further found by Müller *et al.* [26] and Silve *et al.* [27]. These differences infer that the influence of buffer conductivity is highly

dependent on the given configuration. The studies are based on ohmic coupling and do not cover the lower conductivity range of 108–5300 μ S/cm tested here. Determining which trend applies to our setup will determine the suspension conductivity that should be used for subsequent lysis experiments.

Results in Fig. 2 indicate a negative correlation between erythrocyte lysis and solution conductivity when capacitive coupling is introduced. Since dilution also reduces cell concentration, a highly conductive 1:100 dilution with PBS confirms the difference in lysis is due to the conductivity change and not the cell density. This in turn makes lysis of high-density samples feasible if their conductivity can be sufficiently lowered to allow for electric field penetration. A 1:10 dilution of WB remains feasible for leukocyte isolation without such measures (Fig. 2). This data demonstrates that lowering solution conductivity increases the biological impact of a given potential applied via capacitively coupled electrodes. Consequently, subsequent experiments were performed on cell suspensions equilibrated in low conductivity sucrose buffer.

3.3. Leukocyte membrane integrity is preserved during erythrocyte lysis

We proceed to investigate the lysis parameters of WB and leukocyte populations separately prepared from WB (Fig. 3a). A field effect acting on erythrocytes can be observed at 18 V (77.9% lysis) and complete erythrocyte lysis is achieved at 25 V (99.4% lysis). Further increasing the potential to 30 V does not significantly impact lysis of remaining cells (99.5% lysis) because WB also contains a residual fraction of leukocytes. With rising field strength, lysis of the isolated leukocyte population decreases to 77.1% at 40 V. These results reveal a wide window of opportunity for selective enrichment of leukocytes. The lysis curve for leukocytes is unusually shallow and spans over 20 V potential difference or twice the magnitude of lysis onset (Fig. 3a). Other studies find that leukocyte lysis has a much steeper profile and occurs in a narrow window of 1/4th increase in electric field strength from onset of lysis. In a specific instance this range lies between 0.4 and 0.5 kV/cm [10].

These combined findings are in contrast to previous reports on electric-field mediated lysis of WB. Leukocyte lysis typically occurs at a far lower energy threshold than red blood cells, which require up to three times the electric field strength before irreversible electroporation leads to efficient rupture [10]. While previous studies conform to the theoretical background described by equation [1], the presented data suggests an inverse relationship between cell size and lysis threshold.

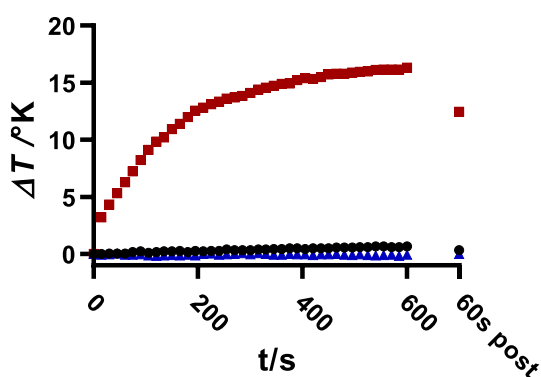


Fig. 1. Temperature drift from starting temperature with 30 V applied continuously at 100 Hz with (●) and without passivation (■) compared to thermometer drift with no field applied (▲). 60 s post: temperature 60 s after the last pulse.

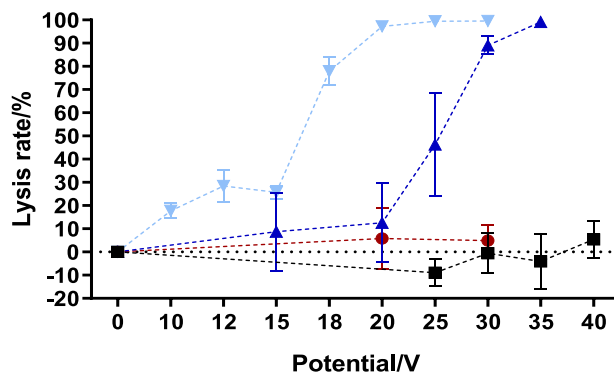


Fig. 2. Voltage dependent lysis rate of various WB dilutions from the same donor. Undiluted: 5109–5300 μ S/cm (■), 1:10: 890 – 920 μ S/cm (▲), 1:100: 108–112 μ S/cm (▼), 1:1000 PBS: 16 000 μ S/cm (●). Conductivity range refers to start and end of the experiment. λ : 100 Hz; flow rate: 100 μ l/min; $n = 3$.

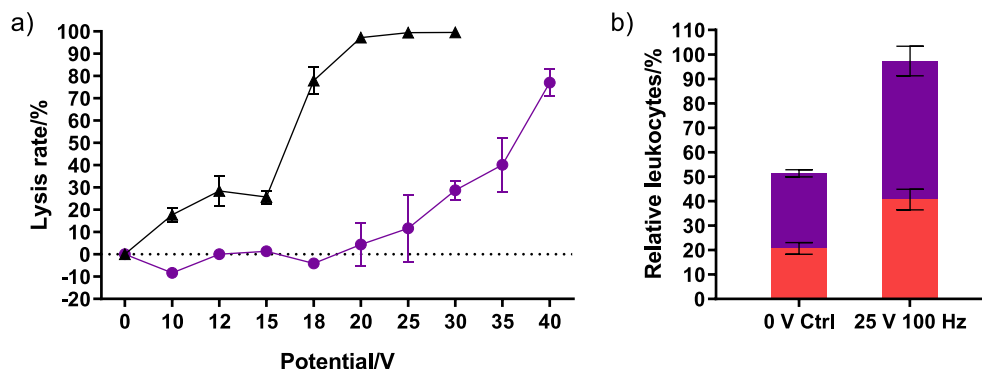


Fig. 3. (a) Voltage-dependent lysis rate of isolated leukocytes (●) in EPB. Erythrocyte lysis (▲) at the same conductivity is taken from Fig. 2 for comparison. 5×10^5 leukocytes/ml in EPB (102–106 $\mu\text{S}/\text{cm}$); λ : 100 Hz; flow rate: 100 $\mu\text{l}/\text{min}$; $n = 3$. (b) Enrichment of leukocytes in a leukocyte spiked WB dilution. Intact: Hoechst 33342 positive (■); Permeabilized: Propidium iodide positive (■); Cell concentrations: 5×10^5 cells/ml; σ : 220–230 $\mu\text{S}/\text{cm}$; $n = 3$.

To further investigate this discrepancy, we proceeded to determine the membrane integrity of cells that appear unaffected in lysis experiments. For this purpose, a spike-in suspension of WB and isolated leukocytes was prepared with a final cell ratio of 1:1. Controls contained 51.4% leukocytes and 48.6% erythrocytes. Conductivity was adjusted to 220 $\mu\text{S}/\text{cm}$ and voltage set to 25 V with all other parameters unchanged. These settings eliminated 94.4% of erythrocytes from the elution, which was comprised of 97.3% remaining leukocytes (Fig. 3b). In the control sample not subjected to an electric field, 40.3% of the leukocytes are PI positive (20.7% of total) indicating membrane aberrations not caused by the electric field. After field application and selective erythrocyte lysis, the fraction of permeabilized leukocytes remains equal (41.7% of leukocytes). This indicates that the applied field has a negligible impact on membrane integrity of leukocytes and serves to support the curious observations from Fig. 3b. These results imply the feasibility of using electric fields toward discrimination of erythrocytes and, consequently, the selective isolation of viable leukocytes.

3.4. Electric field mediated lysis of Jurkat T lymphocytes, MCF-7 and leukocytes is not size dependent when using capacitive coupling

In pertinent literature, the lysis of leukaemia- and circulating tumour cells occurs at thresholds lower than that of the leukocyte population [8,10]. Similarly, Fig. 4a shows that Jurkat T lymphocytes have the highest susceptibility to voltage dependent lysis. Square wave pulses of 15 V result in lysis of 77.4% of Jurkat- and 69.3% of MCF-7 cells. Notably, this means that both cancer models

display a higher field susceptibility than erythrocytes at the same field strength and conductivity (Figs. 2 and 3a, 25.7% lysis). Leukocytes are mainly comprised of neutrophils (7.3–9.7 μm), lymphocytes (5.89–6.09 μm) and monocytes (7.72–9.99 μm) [28]. The diameter of MCF-7 cells ranges from 15 to 17 μm [29] and Jurkat T lymphocytes range from 10 to 13 μm [30]. While erythrocytes are significantly smaller ($7.81 \pm 0.63 \mu\text{m}$) [31] their non-spherical shape could change the dynamics of their susceptibility to electric fields. If cell diameter were the primary factor governing electric field mediated lysis, we would expect to find Jurkat T lymphocyte lysis rate to fall somewhere between the two other examined cell types. Fig. 4b plots the size of tested cell populations against the voltage needed for disruption of 50% of the respective cell type (EV50). Jurkat T lymphocytes show the highest susceptibility to voltage dependent lysis (13.3 V), followed by MCF-7 (13.6 V), erythrocytes (16.9 V) and leukocytes (36.5 V). Fig. 4b shows that the capacitively coupled configuration does not result in the linear, positive correlation between lysis rate and cell size that is suggested by Eq. (1) ($R^2 = 0.249$).

3.5. Capacitive coupling allows for selective elimination of Jurkat T lymphocytes and MCF-7 cells from a mixture with leukocytes

To test whether these effects persist in a mixed-population suspension, spike-in experiments were performed. Fig. 5 shows flow cytometry data with and without field application to a 1:1 mixture of Jurkat T lymphocyte- and leukocyte suspensions. In the mixed population without field application, 31.6% of counted events are Calcein-AM positive Jurkat T lymphocytes and 41.7% are identified

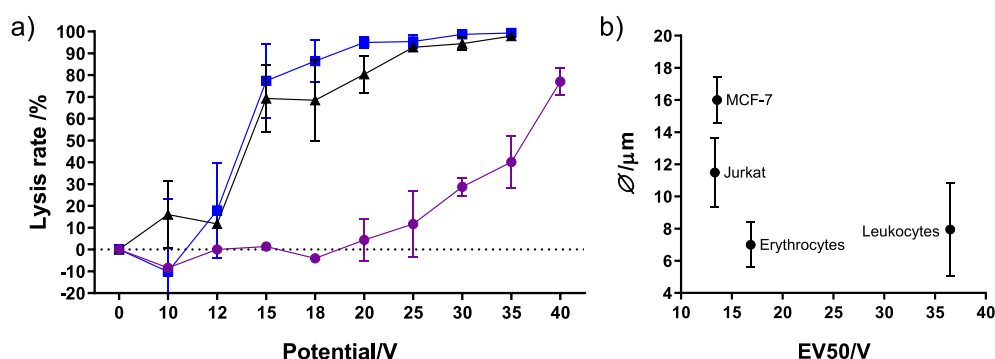


Fig. 4. (a) Lysis rates of Jurkat T lymphocytes (■) and MCF-7 cells (▲) exposed to increasing electric fields at the same conductivity. Leukocyte lysis rate (●) added from Fig. 3a for comparison. All cell concentrations 5×10^5 cells/ml; σ [Jurkat] 107–116 $\mu\text{S}/\text{cm}$, σ [MCF-7] 99–104 $\mu\text{S}/\text{cm}$; Conductivity range refers to start and end of experiment. λ : 100 Hz; flow rate: 100 $\mu\text{l}/\text{min}$; $n = 3$. (b) Average cell size according to literature plotted against effective voltage 50 (EV50), which is the voltage required for lysis of 50% of cells as determined by nonlinear curve fit (Boltzmann-sigmoid).

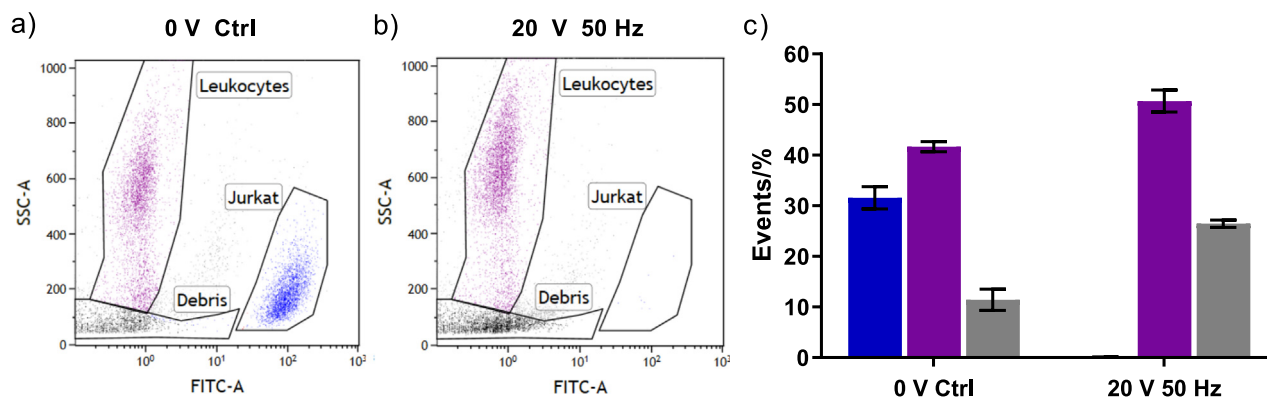


Fig. 5. Selective elimination of Jurkat T lymphocyte population mixed with isolated leukocytes. Jurkat T lymphocytes were incubated with Calcein-AM prior to data acquisition and have high FITC fluorescence. (a) Mixed cell population without electric field application. (b) Mixed cell population after application of 20 V square wave pulses at 50 Hz. (c) Event statistics showing percentage of respective events (Blue: Ca-AM positive Jurkat T lymphocytes, Purple: Leukocytes, Grey: Debris), Conductivity: 97 $\mu\text{S}/\text{cm}$; events: 10 000; data composed from three biological replicates. (For interpretation of the references to colour in this figure legend, the reader is referred to the web version of this article.)

as leukocytes by their SSC profile (Fig. 5a). Upon field application, <0.1% of the events remain Calcein-AM positive Jurkat T lymphocytes while 50.7% of events are accounted to leukocytes (Fig. 5b). Cellular debris increases from 11.4% to 26.5% with field application (Fig. 5b and c). The increase of debris, SSC gating and previous lysis experiments (Fig. 4a) support the notion that Jurkat T lymphocytes undergo lysis instead of losing Calcein-AM fluorescence. The increase in debris suggests that Jurkat T lymphocytes disintegrate to smaller particles in response to the applied field. Fig. 5c shows combined event statistics from multiple experiments. The number of events attributed to unaffected Jurkat cells was below 0.1% in all three repetitions.

Fig. 6a and b show flow cytometry data with and without field application to a 1:1 mixture of MCF-7 and leukocytes. MCF-7 cells were stained with FITC-conjugated antibody for identification. Lysis rate was assessed via Hoechst 33342 addition prior to data acquisition. In the mixed population control, 69.8% of labelled MCF-7 cells were counted as viable with 91.7% of leukocytes remaining intact (Fig. 6a and c). Application of 30 V square wave pulses at 100 Hz result in 97.9% lysis of the MCF-7 population while 68.5% of leukocytes remain intact (Fig. 6b and c). Fig. 6c shows the average population counts for two technical replicates with SD.

High-k dielectric passivation reliably reduces tumour cell count while keeping leukocyte populations intact. In the case of Jurkat T lymphocyte spike-in experiments, the leukocyte count remains virtually unchanged by the applied electric field. The higher energy

pulses of 30 V applied to the MCF-7 leukocyte spike-in results in the death of 21.9% of leukocytes. Affirming the results from Fig. 3a, this emphasizes the consistency and reproducibility of experimental outcome using capacitive coupling. While the standard rationale for leukocyte lysis invokes unspecific side effects due to electrochemistry, this does not serve as an explanation for the observed specificity in this capacitively coupled system where these effects are suppressed [17]. We propose that any such increase in lysis rate is a result of reaching the field threshold necessary for the elimination of the specific subset of leukocytes.

A further proposed mechanism for the specificity of electric field mediated lysis relates to the expansion of affected nuclei and feasibly explains the lower lysis threshold of malignant cells [10]. However, applied to our findings, these features do not reflect the lysis dynamics of erythrocytes compared to the tested leukaemia and circulating tumour cell models. These results stress the necessity of a mechanistic explanation for the dynamics of cell lysis using capacitive coupling of electric fields.

4. Conclusion

The current understanding of electroporation implies a selective component to the interaction of electric fields with lipid double layers. Despite this theoretical selectivity, a practical approach for electric field mediated cell discrimination in liquid samples comprises significant challenges. While tumour ablation in tissues can be achieved in a selective manner by careful configuration of

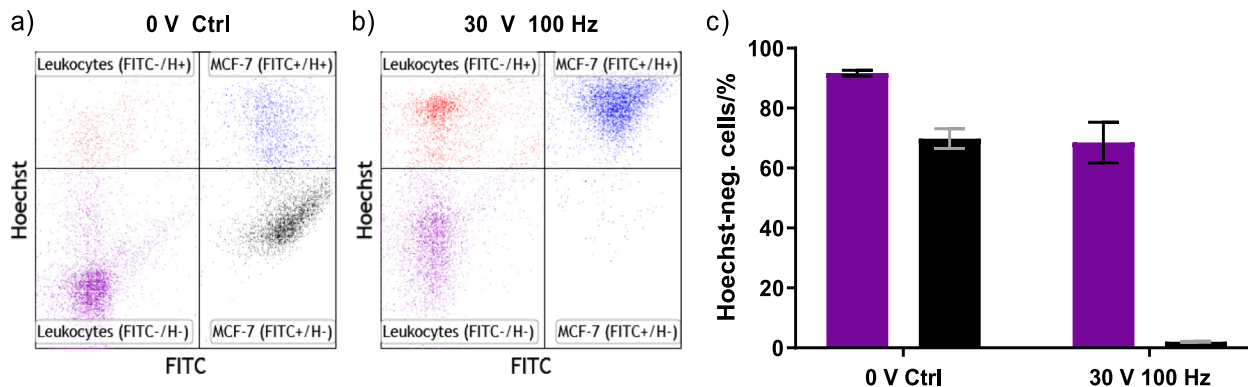


Fig. 6. Selective elimination of MCF-7 cells mixed with leukocyte suspension. (a) Mixed cell populations without electric field. (b) Mixed cell suspension after application of 30 V at 100 Hz. (c) Statistics on lysis upon field application (Purple: Leukocytes, Black: MCF-7) Conductivity: 100–103 $\mu\text{S}/\text{cm}$; events: 10 000; data composed from two biological replicates. (For interpretation of the references to colour in this figure legend, the reader is referred to the web version of this article.)

spatial electrode geometry, no comparable workaround is available for cell suspensions. Suspended cells subjected to electric fields applied with capacitive coupling have a consistent response that results in reproducible outcome with low standard deviation. This enables the selective lysis of specific cell types from a mixture of cells. Surprisingly, the order of lysis observed for the tested cell types does not coincide with pertinent literature. Similar lysis dynamics are observed for MCF-7 and Jurkat cells despite their significant size difference. These and other discussed findings are in conflict with previous reports on the subject and imply a further feature of electric field susceptibility not related to cell radius. This suggests that the potential of selective lysis by electric fields may offer greater flexibility than previously assumed. We are currently invested to reconcile these findings by thorough characterization of the different lysis mechanics between commonly used platforms and capacitively coupled systems.

CRediT authorship contribution statement

Terje Wimberger: Conceptualization, Methodology, Investigation, Writing - original draft, Writing - review & editing, Visualization. **Verena K. Köhler:** Methodology, Investigation, Visualization. **Eva K. Ehmoser:** Conceptualization, Resources, Writing - review & editing, Supervision. **Klemens J. Wassermann:** Conceptualization, Methodology, Investigation, Resources, Writing - review & editing, Supervision, Project administration, Funding acquisition.

Declaration of Competing Interest

We declare that the authors Terje Wimberger and Klemens J. Wassermann have filed a patent application (Date: 12.12.2018; application number: EP18211969.3) on behalf of the Austrian Institute of Technology which includes the following aspects of the manuscript: The passivation strategy, prototype design and its application towards specific cell lysis. Verena K. Köhler and Eva-Kathrin Ehmoser have no conflicts of interest to declare.

Acknowledgement

The authors would like to acknowledge the Austrian Institute of Technology GmbH as the source of funding for this project. Thanks go to the FFG for funding the internship of Verena K. Köhler. We acknowledge Seta Küpcü from the Department of Nanobiotechnology at BOKU University for her support in flow cytometry data acquisition.

Appendix A. Supplementary material

Supplementary data to this article can be found online at <https://doi.org/10.1016/j.bioelechem.2020.107495>.

References

- [1] S. Bae, S. Park, J. Kim, J.S. Choi, K.H. Kim, D. Kwon, E. Jin, I. Park, D.H. Kim, T.S. Seo, Exogenous gene integration for microalgal cell transformation using a nanowire-incorporated microdevice, *ACS Appl. Mater. Interfaces* 7 (49) (2015) 27554–27561, <https://doi.org/10.1021/acsami.5b09964>.
- [2] J.C. Weaver, K.C. Smith, A.T. Esser, R.S. Son, T.R. Gowrishankar, A brief overview of electroporation pulse strength-duration space: a region where additional intracellular effects are expected, *Bioelectrochemistry* (Amsterdam, Netherlands) 87 (2012) 236–243, <https://doi.org/10.1016/j.bioelechem.2012.02.007>.
- [3] M.-P. Rols, J. Teissié, Electroporation of mammalian cells to macromolecules: control by pulse duration, *Biophys. J.* 75 (3) (1998) 1415–1423, [https://doi.org/10.1016/S0006-3495\(98\)74060-3](https://doi.org/10.1016/S0006-3495(98)74060-3).
- [4] C. Rosazza, S.H. Meglic, A. Zumbusch, M.-P. Rols, D. Miklavcic, Gene electrotransfer: a mechanistic perspective, *Curr. Gene Ther.* 16 (2) (2016) 98–129, <https://doi.org/10.2174/1566523216666160331130040>.
- [5] H. Pauly, H.P. Schwan, Über die Impedanz einer Suspension von kugelförmigen Teilchen mit einer Schale; Ein Modell für das dielektrische Verhalten von Zellsuspensionen und von Proteinlösungen, *Zeitschrift für Naturforschung, Teil B, Chemie, Biochemie, Biophysik, Biologie und verwandte Gebiete* 14B (2) (1959) 125–131.
- [6] T. Kotnik, G. Pucihar, D. Miklavcic, Induced transmembrane voltage and its correlation with electroporation-mediated molecular transport, *J. Membr. Biol.* 236 (1) (2010) 3–13, <https://doi.org/10.1007/s00232-010-9279-9>.
- [7] S. Li, Optimizing electrotransfection of Mammalian cells in vitro, *CSH protocols* (2006), 1. 10.1101/pdb.prot4449.
- [8] H.M. Eppich, R. Foxall, K. Gaynor, D. Dombkowski, N. Miura, T. Cheng, S. Silva-Arrieta, R.H. Evans, J.A. Mangano, F.I. Pfeffer, D.T. Scadden, Pulsed electric fields for selection of hematopoietic cells and depletion of tumor cell contaminants, *Nat. Biotechnol.* 18 (8) (2000) 882–887, <https://doi.org/10.1038/78504>.
- [9] A. Craiu, Y. Saito, A. Limon, H.M. Eppich, D.P. Olson, N. Rodrigues, G.B. Adams, D. Dombkowski, P. Richardson, R. Schlossman, P.S. Choi, J. Grogins, P.G. O'Connor, K. Cohen, E.C. Attar, J. Freshman, R. Rich, J.A. Mangano, J.G. Gribben, K.C. Anderson, D.T. Scadden, Flowing cells through pulsed electric fields efficiently purges stem cell preparations of contaminating myeloma cells while preserving stem cell function, *Blood* 105 (5) (2005) 2235–2238, <https://doi.org/10.1182/blood-2003-12-4399>.
- [10] N. Bao, T.T. Le, J.-X. Cheng, C. Lu, Microfluidic electroporation of tumor and blood cells: observation of nucleus expansion and implications on selective analysis and purging of circulating tumor cells, *Integr. Biol. Quant. Biosci. Nano Macro* 2 (2–3) (2010) 113–120, <https://doi.org/10.1039/B919820B>.
- [11] P. Turjanski, N. Olaiz, F. Maglietti, S. Michinski, C. Suarez, F.V. Molina, G. Marshall, The role of pH fronts in reversible electroporation e17303 *PLoS One* 4 (6) (2011), <https://doi.org/10.1371/journal.pone.0017303>.
- [12] J.A. Kim, K. Cho, M.S. Shin, W.G. Lee, N. Jung, C. Chung, J.K. Chang, A novel electroporation method using a capillary and wire-type electrode, *Biosens. Bioelectron.* 23 (9) (2008) 1353–1360, <https://doi.org/10.1016/j.bios.2007.12.009>.
- [13] A. Meir, B. Rubinsky, Alternating electric field capacitively coupled micro-electroporation, *RSC Adv.* 4 (97) (2014) 54603–54613, <https://doi.org/10.1039/C4RA09054C>.
- [14] L. Chopinet, M.-P. Rols, Nanosecond electric pulses: a mini-review of the present state of the art, *Bioelectrochemistry* (Amsterdam, Netherlands) 103 (2015) 2–6, <https://doi.org/10.1016/j.bioelechem.2014.07.008>.
- [15] S. Movahed, D. Li, Microfluidics cell electroporation, *Microfluid. Nanofluid.* 10 (4) (2011) 703–734, <https://doi.org/10.1007/s10404-010-0716-y>.
- [16] T. Geng, C. Lu, Microfluidic electroporation for cellular analysis and delivery, *Lab Chip* 13 (19) (2013) 3803–3821, <https://doi.org/10.1039/c3lc50566a>.
- [17] T. Wimberger, J.R. Peham, E.-K. Ehmoser, K.J. Wassermann, Controllable cell manipulation in a microfluidic pipette-tip design using capacitive coupling of electric fields, *Lab Chip* 19 (23) (2019) 3997–4006, <https://doi.org/10.1039/C9LC00927B>.
- [18] H. Shafiee, J.L. Caldwell, M.B. Sano, R.V. Davalos, Contactless dielectrophoresis: a new technique for cell manipulation, *Biomed. Microdevices* 11 (5) (2009) 997–1006, <https://doi.org/10.1007/s10544-009-9317-5>.
- [19] M.B. Sano, J.L. Caldwell, R.V. Davalos, Modeling and development of a low frequency contactless dielectrophoresis (cDEP) platform to sort cancer cells from dilute whole blood samples, *Biosens. Bioelectron.* 30 (1) (2011) 13–20, <https://doi.org/10.1016/j.bios.2011.07.048>.
- [20] K.J. Wassermann, S. Barth, F. Keplinger, C. Noehammer, J.R. Peham, High-k dielectric passivation: novel considerations enabling cell specific lysis induced by electric fields, *ACS Appl. Mater. Interfaces* 8 (33) (2016) 21228–21235, <https://doi.org/10.1021/acsami.6b06927>.
- [21] S.R.A. Kratz, C. Eilenberger, P. Schuller, B. Bachmann, S. Spitz, P. Ertl, M. Rothbauer, Characterization of four functional biocompatible pressure-sensitive adhesives for rapid prototyping of cell-based lab-on-a-chip and organ-on-a-chip systems, *Sci. Rep.* 9 (1) (2019), <https://doi.org/10.1038/s41598-019-45633-x>.
- [22] B.M. Novac, F. Banakhr, I.R. Smith, L. Pecastaing, R. Ruscassie, A. de Ferron, P. Pignolet, Y. Liu, Non-invasive pulsed electric field food processing: Proof-of-principle experiments, in: 2012 IEEE International Power Modulator and High Voltage Conference (IPMHVC), IEEE, 03-Jun-12 - 07-Jun-12, pp. 528–531. 10.1109/IPMHVC.2012.6518797.
- [23] G. Pucihar, T. Kotnik, M. Kanduser, D. Miklavcic, The influence of medium conductivity on electroporation and survival of cells in vitro, *Bioelectrochemistry* (Amsterdam, Netherlands) 54 (2) (2001) 107–115, [https://doi.org/10.1016/S1567-5394\(01\)00117-7](https://doi.org/10.1016/S1567-5394(01)00117-7).
- [24] A. Ivorra, J. Villemejane, Lluís M. Mir, Electrical modeling of the influence of medium conductivity on electroporation, *Phys. Chem. Chem. Phys.* 12 (2010) 10055–10064, <https://doi.org/10.1039/c004419a>.
- [25] C.S. Djuzenova, U. Zimmermann, H. Frank, V.L. Sukhorukov, E. Richter, G. Fuhr, Effect of medium conductivity and composition on the uptake of propidium iodide into electroporated myeloma cells, *Biochim. Biophys. Acta (BBA) - Biomembr.* 1284 (2) (1996) 143–152, [https://doi.org/10.1016/S0005-2736\(96\)00119-8](https://doi.org/10.1016/S0005-2736(96)00119-8).
- [26] K.J. Müller, V.L. Sukhorukov, U. Zimmermann, Reversible electroporation of mammalian cells by high-intensity, ultra-short pulses of submicrosecond duration, *J. Membr. Biol.* 184 (2) (2001) 161–170, <https://doi.org/10.1007/s00232-001-0084-3>.
- [27] A. Silve, I. Leray, C. Poignard, L.M. Mir, Impact of external medium conductivity on cell membrane electroporation by microsecond and nanosecond electric pulses, *Sci. Rep.* 6 (2016) 19957, <https://doi.org/10.1038/srep19957>.

- [28] G.P. Downey, D.E. Doherty, B. Schwab, E.L. Elson, P.M. Henson, G.S. Worthen, Retention of leukocytes in capillaries: role of cell size and deformability, *J. Appl. Physiol.* (Bethesda, Md. 1985) 69 (1990), <https://doi.org/10.1152/jappl.1990.69.5.1767>.
- [29] R. Milo, P. Jorgensen, U. Moran, G. Weber, M. Springer, BioNumbers—the database of key numbers in molecular and cell biology, *Nucleic Acids Res.* 38 (2010), <https://doi.org/10.1093/nar/gkp889>, Database Issue pp. D750–753.
- [30] M.J. Rosenbluth, W.A. Lam, D.A. Fletcher, Force microscopy of nonadherent cells: a comparison of leukemia cell deformability, *Biophys. J.* 90 (8) (2006) 2994–3003, <https://doi.org/10.1529/biophysj.105.067496>.
- [31] M.E. Fabry, D.K. Kaul, C. Raventos, S. Baez, R. Rieder, R.L. Nagel, Some aspects of the pathophysiology of homozygous Hb CC erythrocytes, *J. Clin. Investig.* 67 (5) (1981) 1284–1291, <https://doi.org/10.1172/JCI110156>.

3. Discussion

From our published findings on cell manipulation using capacitive coupling, two major divergences from classic electroporation have remained unaddressed; The theoretical background of the empirical requirement for incredibly low buffer conductivities and the order of lysis susceptibility between different cell types remain puzzling. The following discussion aims to address some of the possible, underlying phenomena.

3.1 Electrodynamic implications

Several electrodynamic characteristics of the passivated system are explained in an applied physics paper by Morrow and colleagues, describing the reaction of a salt solution upon electric field exposure.[80] A few especially interesting points made in this study can help us to understand the influence of conductivity in electroporation using capacitive coupling. Figure 8A shows the relevance of this model when applied to our findings. When charge transfer is neglected, the current dynamics modeled for the ionic solution corresponds exactly to our experimental measurements. While calculations are performed for potentials in the mV range, extrapolating these trends to the voltages used in our own publications reveals that a lower conductivity will result in a longer pulse affecting the bulk solution. This happens for two reasons; First, low conductivities significantly increase the Debye length and thereby the travel time during charge separation. Disregarding the phosphate component of our electroporation buffer, the addition of 1 mM NaCl results in a large calculated Debye length of about 9.6 nm. Second, since the shape of the double layer is defined by Debye length and must remain equal regardless of voltage, a potential increase must be accompanied by increased ionic accumulation. For this reason, a voltage increment also lengthens the time until equilibrium is reached.[80] Remembering that an equilibrium in capacitive coupling means that the bulk electric field is zero, we discover why the biologically relevant pulse length has an inverse correlation to solution conductivity. This would mean that the inverse correlation between field strength and conductivity observed in both publications is due to a longer pulse duration acting on suspended cells.

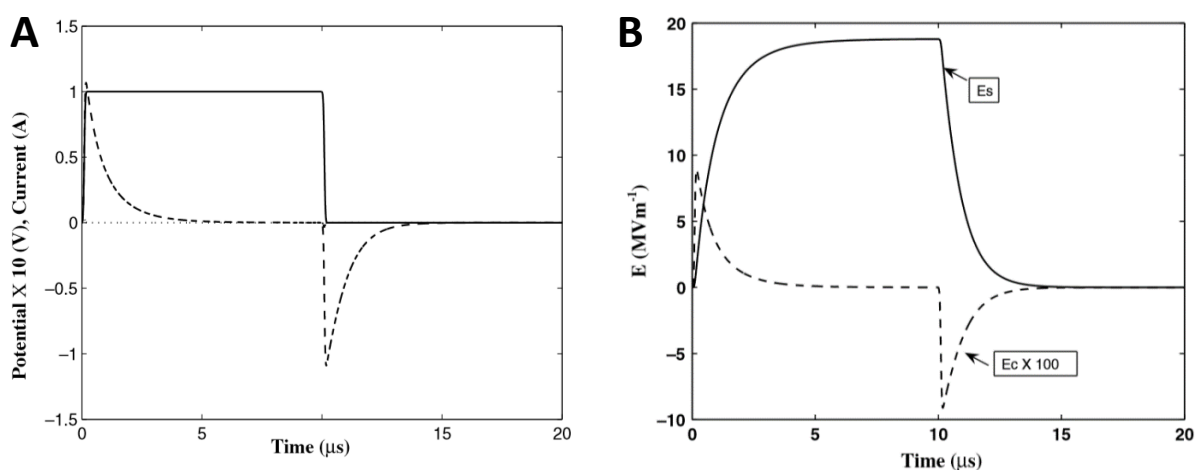


Figure 8 (A) Voltage (—), current (---) and displacement current (···) waveforms computed for 20 μs of a 10 μs rectangular pulses applied to blocking electrodes with a rise time of 100 ns. (B) Development of the electric field as a result of the same pulse 0.03 nm from the anode (E_s) and 500 nm from the anode, considered at the center of the saline solution (E_c). Morrow 2006 *Journal of Physics D: Applied Physics* [80]

Figure 8B combines spatial- and time-resolved field distributions. While the initial electric field in the bulk (E_c) is large at onset of pulse application, it quickly decays in the μs-timescale until an electric field

measuring 1/100th of the initial bulk magnitude becomes confined to a few nanometers of interface (E_s).

When transferring these insights to our own technology, perhaps the most intriguing aspect of the paper is that a pulse rise-time of 100 ns was chosen. The authors specifically state that the magnitude of displacement current would be much greater for a short rise time, which is the case for the presented capacitive coupling electroporation strategy. We recognize that our design (large area to volume ratio) coupled with high-k passivation (strong dielectric) and rectangular pulses (of rise-times around 1 ns as determined by steepness of periodic current spikes) fulfills all criteria that typically result in a large contribution of displacement current during capacitive charging.[80,82] This has two possible implications of undetermined significance. First, our conclusions of cell lysis dynamics assume a situation without displacement current as shown in figure 8. The real contribution of displacement current as part of the measured total current is unknown and might bias our perceived understanding of how current peaks relate to cell manipulation. Second, the magnitude of displacement current would be proportional to a magnetic field that significantly penetrates the electroporation buffer as displayed in purple for the anodic side in figure 9. It would be expected to act perpendicular to the electric field inside the electroporation buffer. This in turn allows for the possibility of an externally induced electric field at the relaxed poles of affected cells, acting geometrically perpendicular to the membrane.

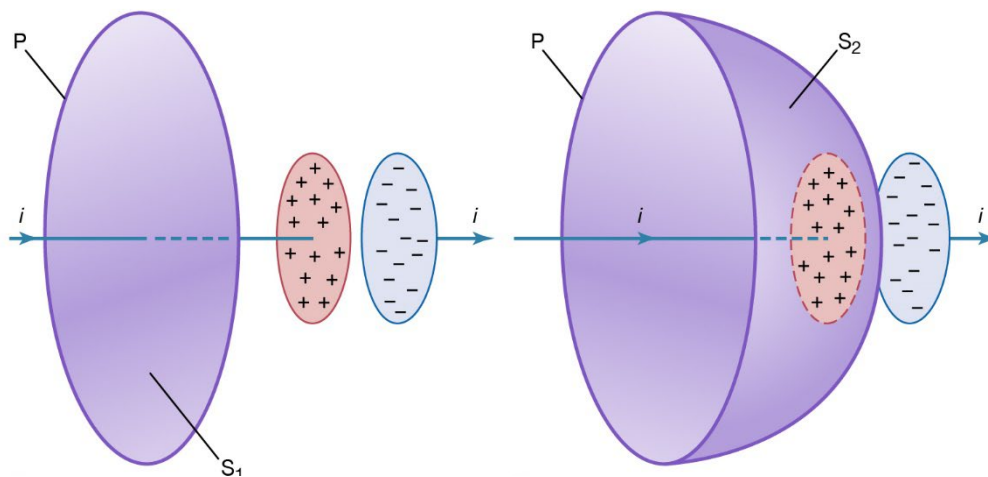


Figure 9 Current charging a capacitor, illustrating Maxwell's displacement current. P: path of magnetic field, i: direction of current, $S_{1/2}$: respective magnetic field surface. *Kashy et. al. 2020, Encyclopaedia Britannica – Effects of Varying Electric Fields*

3.2 Biological implications

As stated in the conclusion of the second publication in section 2.2, cell specific lysis in capacitive coupling is not only highly selective but displays a type of specificity that deviates from pertinent literature. Comparing the voltage-dependent lysis dynamics of different cell types, we find no correlation to cell size or literature measurements for membrane capacitance (unpublished), the two core dependencies proposed by the Schwann equation (1). The non-correlation between lysis and cell diameter was experimentally demonstrated by flow cytometry forward-scatter measurements in section 2.2. The relationship $V_m = Q / C_m$ between membrane voltage (V_m), charge (Q) and membrane capacitance (C_m) suggests that a smaller capacitance will increase the transmembrane voltage induced by a constant amount of charge. However, derivation of membrane capacitance poses significant challenges due to the complex dependencies of this characteristic,[83] exemplified by literature values for specific lineages differing by up to 100% depending on measurement conditions. (i.e. HEK-293: [11,84] MCF-7, Leukocytes: [85,86]) In addition, measurements of total membrane capacitance can be

misleading because these values increase with cell size. Since electroporation occurs locally and perpendicular to the electric field, the relevant capacitance per lipid membrane area is of greater interest but even harder to measure dynamically.[83] Further, any magnitude of membrane capacity at resting potential can be equally misleading due to the voltage dependency of the property itself,[87] with lower voltages correlating with a stronger increase in capacity of the lipid bilayer.[88] Further adding frequency dependent behavior [89] to its range of co-dependencies negates the practical applicability of membrane capacitance as a predictive lysis indicator. A further cellular property that is heavily influenced by medium composition is the resting transmembrane potential. For physiological salt compositions it can be calculated using the Goldman equation.[90] Physiological membrane potentials vary between -8 mV for erythrocytes [91] down to <-90 mV in skeletal muscle cells,[92] with epithelial cells such as HEK-293 measuring around -50 mV [93] at physiological conditions. Solving the Goldman equation for a generic mammalian cell suspended in a 160 $\mu\text{S}/\text{cm}$ electroporation buffer prepared from diluted PBS results in predicted values below -90 mV.[94] The calculated electrochemical driving forces acting on ionic components measure up to 400 mV, suggesting increased ion-channel flux across the membrane even without an external field component. This implies that the resting transmembrane potential is subject to dynamic change while a cell is suspended in the electroporation buffer. Empirically, dwelling time in the electroporation buffer causes negligible viability loss (first publication, section 2.2) and does not impact field-mediated lysis dynamics even after 2 hours of exposure to low conductivities (unpublished). A further biological explanation for higher electric field effects at low conductivities could be attributed to a shorter membrane charging time.[95] This property describes how long it takes the respective membrane to return to its resting state. Since the membrane time constant is in turn the product of membrane capacitance and membrane resistance, we are left with the latter term as a potential predictive indicator for the field susceptibility of cells. Recalling Ohm's law, we recognize that a higher membrane resistance means that less current is required to maintain or change a given voltage.[96] Since membrane resistance is primarily determined by ion channel prevalence, there is an inclination toward an indicative biological trait that determines how fast a cell can react to its initial polarization. However, the amount and conductance of ion channels is expected to be similarly heterogeneous- and challenging to interpret as membrane capacitance itself. A more intuitive explanation for increased biological field effects in low conductivity media is invoked by revisiting section 1.3. of the introduction. When an external electric field of sufficient magnitude results in dielectric breakdown of the membrane, hydrophilic pore formation reduces the effective membrane resistance far below resting magnitude. Since the conductivity of a pore must be proportional to the surrounding medium, a lower ion concentration will reduce the rate of charge flux that leads to membrane relaxation. This means the same as an increase of the effective membrane charging time and thereby the time required for pore closure.[97] We are left with the hypothesis that a low solution conductivity might simply lower the rate of pore closure and thereby facilitates pore expansion during sustained field application. Few cellular processes that are expected during homeostasis or even chemical stimulation will have a larger impact on the electric- and dielectric properties of a complex lipid bilayer than electroporation conditions above a critical breakdown threshold. This explains why existing measurements of resting states may have limited predictive significance to the observed order of field-mediated cell lysis in such dynamic processes.

4. Conclusion and outlook

The featured publications demonstrate a formidable spectrum of improvements to classic electroporation processes that are directly linked to the introduction of electrode passivation. The demonstrable reduction of charge transfer between liquid and electrode (first publication, section 2.1) increases biological consistency and reveals precise dependencies to pertinent variables (sections 2.2-2.4). Both findings are reiterated in the second manuscript for an entirely different model, showcasing their universal applicability. Results of the latter publication along with a growing arsenal of inexplicable, unpublished data reveals that a thorough understanding of the underlying mechanisms remains out of reach. Observed lysis dynamics for red, white and malignant blood cells are unparalleled in pertinent literature with respect to both order and degree of specificity. Since what we have learned enables us to ask the right questions, manuscripts and proposals are in preparation for both topics of the prior discussion. An exhaustive electrodynamic model must include the relationship between all demonstrated biological effects and the dielectric constant of the passivation layer. Such experiments may confirm or falsify our assumptions concerning electric field effects inside the liquid. Biological implications of field application are currently being compared between a growing number of cell types with varying electroporation buffer compositions. This growing data collection is expected to yield a novel hypothesis concerning the field susceptibility of individual cell populations in capacitive coupling. Finally, the following image is a composite of an oscilloscope measurement from a passivated prototype (Fig. 10A), the computed voltage-current plot for an NaCl solution exposed to an electric field by blocking electrodes (Fig. 10B) and a basic schematic of the electrical properties of a plasma membrane during voltage clamping (Fig. 10C). A single pulse applied via passivated electrodes will simultaneously produce all three identical shapes at their respective interface, although voltage and current slopes may be reversed. We propose that the natural similarity between these interfacial dynamics are at the root of any unique features observed with electric fields applied via capacitive coupling.

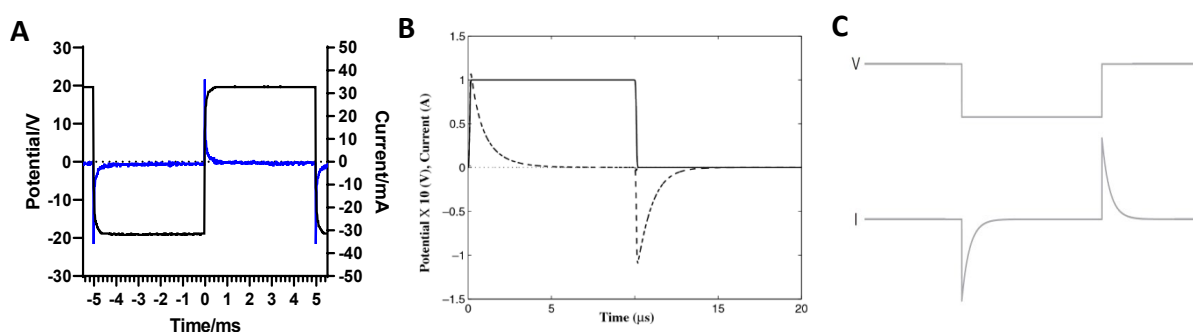


Figure 10 Composite of three related figures. (A) Voltage (black) and current (blue) characteristics of a passivated electric cell lysis unit when 20 V are applied to a 100 mS/cm solution of electroporation buffer at 100 Hz. *Wimberger et. al. 2020 Bioelectrochemistry* [60] (B) Voltage (-----), current (- - -) and displacement current (· · ·) waveforms computed for 20 μ s of a 10 μ s rectangular pulse applied to blocking electrodes with a rise time of 100 ns. *Morrow 2006 Journal of Physics D: Applied Physics* [80] (C) Traces show a voltage step (top) and its current response (bottom) for voltage clamping of a plasma membrane. *Götz and Wilms in Scientifica – Understanding the cell as an electrical circuit* [96]

5. References

- [1] C. Rosazza, S.H. Meglic, A. Zumbusch, M.-P. Rols, D. Miklavcic, Gene Electrotransfer: A Mechanistic Perspective, *Current gene therapy* 16 (2016) 98–129.
- [2] H. Doevenspeck, Verfahren und Vorrichtung zur Gewinnung der einzelnen Phasen aus dispersen Systemen. (1960)
- [3] S. Toepfl, V. Heinz, D. Knorr, High intensity pulsed electric fields applied for food preservation, *Chemical Engineering and Processing: Process Intensification* 46 (2007) 537–546.
- [4] A. Sale and W. Hamilton, Effects of high electric fields on microorganismsI. Killing of bacteria and yeasts, *Biochimica et Biophysica Acta (BBA) - General Subjects* 148 (1967) 781–788.
- [5] W. Hamilton and A. Sale, Effects of high electric fields on microorganismsII. Mechanism of action of the lethal effect, *Biochimica et Biophysica Acta (BBA) - General Subjects* 148 (1967) 789–800.
- [6] A. Sale and W. Hamilton, Effects of high electric fields on micro-organisms, *Biochimica et Biophysica Acta (BBA) - Biomembranes* 163 (1968) 37–43.
- [7] H. Hülshager, J. Potel, E.G. Niemann, Electric field effects on bacteria and yeast cells, *Radiation and environmental biophysics* 22 (1983) 149–162.
- [8] E. Neumann, The Relaxation Hysteresis of Membrane Electroporation, in: E. Neumann, A.E. Sowers, C.A. Jordan (Eds.), *Electroporation and Electrofusion in Cell Biology*, Springer US, Boston, MA, (1989) 61–82.
- [9] 2nd International Conference on Bioinformatics and Biomedical Engineering, IEEE, 16-May-08 - 18-May-08.
- [10] S.J. Beebe, Considering effects of nanosecond pulsed electric fields on proteins, *Bioelectrochemistry (Amsterdam, Netherlands)* 103 (2015) 52–59.
- [11] L.J. Gentet, G.J. Stuart, J.D. Clements, Direct Measurement of Specific Membrane Capacitance in Neurons, *Biophysical journal* 79 (2000) 314–320.
- [12] G.G. Matthews (Ed.), *Cellular Physiology of Nerve and Muscle*, Blackwell Publishing Ltd, Malden, MA USA, 2002.
- [13] T.J. Lewis, A model for bilayer membrane electroporation based on resultant electromechanical stress, *IEEE Trans. Dielect. Electr. Insul.* 10 (2003) 769–777.
- [14] H.T. Tien, A. Ottova, The bilayer Lipid membrane BLM under electrical fields, *IEEE Trans. Dielect. Electr. Insul.* 10 (2003) 717–727.
- [15] D. Casares, P.V. Escribá, C.A. Rosselló, Membrane Lipid Composition: Effect on Membrane and Organelle Structure, Function and Compartmentalization and Therapeutic Avenues, *International journal of molecular sciences* 20 (2019).
- [16] F. Conti, W.E. Blumberg, J. de Gier, F. Pocchiari (Eds.), *Physical Methods on Biological Membranes and Their Model Systems*, Springer US, Boston, MA, 1985.
- [17] D.C. Chang, *Guide to Electroporation and Electrofusion*, Elsevier Science, Burlington, 2012.
- [18] G. Saulis, M.S. Venslauskas, Cell electroporation, *Bioelectrochemistry and Bioenergetics* 32 (1993) 221–235.

- [19] C. Chen, S.W. Smye, M.P. Robinson, J.A. Evans, Membrane electroporation theories: a review, *Medical & biological engineering & computing* 44 (2006) 5–14.
- [20] S.A. Kirsch, R.A. Bockmann, Membrane pore formation in atomistic and coarse-grained simulations, *Biochimica et biophysica acta* 1858 (2016) 2266–2277.
- [21] S.Y. Ho, G.S. Mittal, Electroporation of cell membranes: a review, *Critical reviews in biotechnology* 16 (1996) 349–362.
- [22] W. Krassowska, P.D. Filev, Modeling electroporation in a single cell, *Biophysical journal* 92 (2007) 404–417.
- [23] G. Saulis, R. Saulė, Size of the pores created by an electric pulse: microsecond vs millisecond pulses, *Biochimica et biophysica acta* 1818 (2012) 3032–3039.
- [24] G. Saulis, Cell electroporation: estimation of the number of pores and their sizes, *Biomedical sciences instrumentation* 35 (1999) 291–296.
- [25] T. Kotnik, L. Rems, M. Tarek, D. Miklavčič, Membrane Electroporation and Electropermeabilization: Mechanisms and Models, *Annual review of biophysics* 48 (2019) 63–91.
- [26] Z.-Y. Huo, J.-F. Zhou, Y. Wu, Y.-H. Wu, H. Liu, N. Liu, H.-Y. Hu, X. Xie, A Cu₃P nanowire enabling high-efficiency, reliable, and energy-efficient low-voltage electroporation-inactivation of pathogens in water, *J. Mater. Chem. A* 6 (2018) 18813–18820.
- [27] W. Zhao, R. Yang, Y. Gu, C. Li, Effects of pulsed electric fields on cytomembrane lipids and intracellular nucleic acids of *Saccharomyces cerevisiae*, *Food Control* 39 (2014) 204–213.
- [28] G. Cebrián, N. Sagarzazu, R. Pagán, S. Condón, P. Mañas, Heat and pulsed electric field resistance of pigmented and non-pigmented enterotoxigenic strains of *Staphylococcus aureus* in exponential and stationary phase of growth, *International journal of food microbiology* 118 (2007) 304–311.
- [29] J.H. Rossmeisl, P.A. Garcia, T.E. Pancotto, J.L. Robertson, N. Henao-Guerrero, R.E. Neal, T.L. Ellis, R.V. Davalos, Safety and feasibility of the NanoKnife system for irreversible electroporation ablative treatment of canine spontaneous intracranial gliomas, *Journal of neurosurgery* 123 (2015) 1008–1025.
- [30] M. Greiner, S. Cheeks, AngioDynamics Receives FDA Approval to Initiate NanoKnife® DIRECT Clinical Study for the Treatment of Stage III Pancreatic Cancer, 01.04.19.
- [31] H.M. Eppich, R. Foxall, K. Gaynor, D. Dombkowski, N. Miura, T. Cheng, S. Silva-Arrieta, R.H. Evans, J.A. Mangano, F.I. Preffer, D.T. Scadden, Pulsed electric fields for selection of hematopoietic cells and depletion of tumor cell contaminants, *Nature biotechnology* 18 (2000) 882–887.
- [32] A. Craiu, Y. Saito, A. Limon, H.M. Eppich, D.P. Olson, N. Rodrigues, G.B. Adams, D. Dombkowski, P. Richardson, R. Schlossman, P.S. Choi, J. Grogins, P.G. O'Connor, K. Cohen, E.C. Attar, J. Freshman, R. Rich, J.A. Mangano, J.G. Gribben, K.C. Anderson, D.T. Scadden, Flowing cells through pulsed electric fields efficiently purges stem cell preparations of contaminating myeloma cells while preserving stem cell function, *Blood* 105 (2005) 2235–2238.
- [33] N. Bao, T.T. Le, J.-X. Cheng, C. Lu, Microfluidic electroporation of tumor and blood cells: observation of nucleus expansion and implications on selective analysis and purging of circulating tumor cells, *Integrative biology quantitative biosciences from nano to macro* 2 (2010) 113–120.

- [34] L. Rems, M. Ušaj, M. Kanduđer, M. Reberšek, D. Miklavčič, G. Pucihar, Cell electrofusion using nanosecond electric pulses, *Scientific reports* 3 (2013) 3382.
- [35] J. Teissié, C. Ramos, Correlation between Electric Field Pulse Induced Long-Lived Permeabilization and Fusogenicity in Cell Membranes, *Biophysical journal* 74 (1998) 1889–1898.
- [36] K. Imura, Y. Ueda, T. Hayashi, T. Itoh, K. Shimizu, H. Tamai, Y. Yano, K. Naito, J. Kohara, K. Nakane, Y. Matsuura, A. Takeda, T. Takeda, K. Kawai, H. Yamagishi, Induction of cytotoxic T lymphocytes against human cancer cell lines using dendritic cell-tumor cell hybrids generated by a newly developed electrofusion technique, *Int J Oncol* (2006).
- [37] M.M. Sadik, J. Li, J.W. Shan, D.I. Shreiber, H. Lin, Quantification of propidium iodide delivery using millisecond electric pulses: experiments, *Biochimica et biophysica acta* 1828 (2013) 1322–1328.
- [38] Yu 2014.01 Quantification of propidium iodide delivery with millisecond electric pulses A model study. 1828-4 (2013) 1322-1328
- [39] O.N. Pakhomova, B. Gregory, I. Semenov, A.G. Pakhomov, Calcium-mediated pore expansion and cell death following nanoelectroporation, *Biochimica et biophysica acta* 1838 (2014) 2547–2554.
- [40] A. Zielichowska, M. Daczewska, J. Saczko, O. Michel, J. Kulbacka, Applications of calcium electroporation to effective apoptosis induction in fibrosarcoma cells and stimulation of normal muscle cells, *Bioelectrochemistry (Amsterdam, Netherlands)* 109 (2016) 70–78.
- [41] L.G. Campana, S. Mocellin, M. Basso, O. Puccetti, G.L. de Salvo, V. Chiarion-Sileni, A. Vecchiato, L. Corti, C.R. Rossi, D. Nitti, Bleomycin-based electrochemotherapy: clinical outcome from a single institution's experience with 52 patients, *Annals of surgical oncology* 16 (2009) 191–199.
- [42] S. Valpione, L.G. Campana, J. Pigozzo, V. Chiarion-Sileni, Consolidation electrochemotherapy with bleomycin in metastatic melanoma during treatment with dabrafenib, *Radiology and oncology* 49 (2015) 71–74.
- [43] L. Kaestner, A. Scholz, P. Lipp, Conceptual and technical aspects of transfection and gene delivery, *Bioorganic & medicinal chemistry letters* 25 (2015) 1171–1176.
- [44] M. Pavlin, M. Kanduđer, New insights into the mechanisms of gene electrotransfer--experimental and theoretical analysis, *Scientific reports* 5 (2015) 9132.
- [45] T.K. Kim, J.H. Eberwine, Mammalian cell transfection: the present and the future, *Analytical and bioanalytical chemistry* 397 (2010) 3173–3178.
- [46] L. Wang, S.E. Miller, F. Yuan, Ultrastructural Analysis of Vesicular Transport in Electrotransfection, *Microscopy and microanalysis the official journal of Microscopy Society of America, Microbeam Analysis Society, Microscopical Society of Canada* 24 (2018) 553–563.
- [47] R. Rennie, J. Law (Eds.), *A dictionary of chemistry*, Oxford University Press, Oxford, 2016.
- [48] J. Li, W. Tan, M. Yu, H. Lin, The effect of extracellular conductivity on electroporation-mediated molecular delivery, *Biochimica et biophysica acta* 1828 (2013) 461–470.
- [49] L. Su, X. Liao, Z. Huang, A theoretical study on resistance of electrolytic solution: Measurement of electrolytic conductivity, *Results in Physics* 13 (2019) 102274.

- [50] C.-W. Sun and S.-S. Hsiau, Effect of Electrolyte Concentration Difference on Hydrogen Production during PEM Electrolysis 9 (2018) 99–108.
- [51] P.G. Barghouth, M. Thiruvalluvan, N.J. Oviedo, Bioelectrical regulation of cell cycle and the planarian model system, *Biochimica et biophysica acta* 1848 (2015) 2629–2637.
- [52] C.S. Djuzenova, U. Zimmermann, H. Frank, V.L. Sukhorukov, E. Richter, G. Fuhr, Effect of medium conductivity and composition on the uptake of propidium iodide into electroporated myeloma cells, *Biochimica et Biophysica Acta (BBA) - Biomembranes* 1284 (1996) 143–152.
- [53] B. Bhattacharyya, Electrochemical Machining, in: Bijoy Bhattacharyya (Ed.), *Electrochemical Micromachining for Nanofabrication, MEMS and Nanotechnology*, Elsevier, 2015, pp. 25–52.
- [54] A.S. Tijani, N.A. Binti Kamarudin, F.A. Binti Mazlan, Investigation of the effect of charge transfer coefficient (CTC) on the operating voltage of polymer electrolyte membrane (PEM) electrolyzer, *International Journal of Hydrogen Energy* 43 (2018) 9119–9132.
- [55] J.W. Loomis-Husselbee, P.J. Cullen, R.F. Irvine, A.P. Dawson, Electroporation can cause artefacts due to solubilization of cations from the electrode plates. Aluminum ions enhance conversion of inositol 1,3,4,5-tetrakisphosphate into inositol 1,4,5-trisphosphate in electroporated L1210 cells, *The Biochemical journal* 277 (Pt 3) (1991) 883–885.
- [56] C.-C. Chang, M. Mao, Y. Liu, M. Wu, T. Vo-Dinh, F. Yuan, Improvement in Electrotransfection of Cells Using Carbon-Based Electrodes, *Cellular and molecular bioengineering* 9 (2016) 538–545.
- [57] J.C. Weaver, K.C. Smith, A.T. Esser, R.S. Son, T.R. Gowrishankar, A brief overview of electroporation pulse strength-duration space: a region where additional intracellular effects are expected, *Bioelectrochemistry (Amsterdam, Netherlands)* 87 (2012) 236–243.
- [58] G. Pataro, M. Falcone, G. Donsì, G. Ferrari, Metal release from stainless steel electrodes of a PEF treatment chamber: Effects of electrical parameters and food composition, *Innovative Food Science & Emerging Technologies* 21 (2014) 58–65.
- [59] L. Rubinsky, E. Guenther, P. Mikus, M. Stehling, B. Rubinsky, Electrolytic Effects During Tissue Ablation by Electroporation, *Technology in cancer research & treatment* 15 (2016) NP95–NP103.
- [60] T. Wimberger, V.K. Köhler, E.K. Ehmoser, K.J. Wassermann, Capacitive coupling increases the accuracy of cell-specific tumour disruption by electric fields, *Bioelectrochemistry (Amsterdam, Netherlands)* 134 (2020) 107495.
- [61] S. Dzekunov, N. Chopas, L. Li, Methods and devices related to a regulated flow electroporation chamber: US Patent C12M35/02, 2017.
- [62] Lonza Cologne GmbH, Amaxa™ Nucleofector™: 96-well Shuttle™ System Manual, 2009, http://bio.lonza.com/uploads/tx_mwaxmarketingmaterial/Lonza_ManualsProductInstructions_Amaxa_Nucleofector_96-well_Shuttle_System_Manual.pdf, accessed 16 July 2020.
- [63] J.A. Kim, K. Cho, M.S. Shin, W.G. Lee, N. Jung, C. Chung, J.K. Chang, A novel electroporation method using a capillary and wire-type electrode, *Biosensors & bioelectronics* 23 (2008) 1353–1360.
- [64] G. Saulis, R. Lape, R. Praneviciūte, D. Mickevicius, Changes of the solution pH due to exposure by high-voltage electric pulses, *Bioelectrochemistry (Amsterdam, Netherlands)* 67 (2005) 101–108.

- [65] T. Geng, Y. Zhan, J. Wang, C. Lu, Transfection of cells using flow-through electroporation based on constant voltage, *Nature protocols* 6 (2011) 1192–1208.
- [66] Pawel Jerzy Wojcik, Redox.me working electrode compositions, <https://redox.me/collections/all>. Accessed 03.08.2020
- [67] P.M. Meserol, Flow electroporation chamber and method: US Patent F25B21/02, 1998.
- [68] L.P. Zharkova, I.V. Romanchenko, M.A. Buldakov, P.V. Pripitnev, M.A. Bolshakov, V.V. Rostov, Mitochondrial Membrane Permeability After Nanosecond Electromagnetic Pulsed Exposure, in: *ISHCE 2018: 20th International Symposium on High-Current Electronics*, pp. 158–161.
- [69] J.A. Kim, K. Cho, Y.S. Shin, N. Jung, C. Chung, J.K. Chang, A multi-channel electroporation microchip for gene transfection in mammalian cells, *Biosensors & bioelectronics* 22 (2007) 3273–3277.
- [70] C. Church, J. Zhu, G. Huang, T.-R. Tzeng, X. Xuan, Integrated electrical concentration and lysis of cells in a microfluidic chip, *Biomicrofluidics* 4 (2010) 44101.
- [71] Wassermann, 1st World Congress on Electroporation and Pulsed Electric Fields in Biology, Medicine and Food & Environmental Technologies (WC 2015): Portoroz, Slovenia, September 6–10, 2015, Springer, Singapore, Heidelberg, 2016.
- [72] J. Tatum, Electricity and Magnetism: Capacitors. Mixed Dielectrics. [https://phys.libretexts.org/Bookshelves/Electricity_and_Magnetism/Book%3A_Electricity_and_Magnetism_\(Tatum\)/05%3A_Capacitors/5.14%3A__Mixed_Dielectrics](https://phys.libretexts.org/Bookshelves/Electricity_and_Magnetism/Book%3A_Electricity_and_Magnetism_(Tatum)/05%3A_Capacitors/5.14%3A__Mixed_Dielectrics), accessed 11.08.2020
- [73] A. Wypych, I. Bobowska, M. Tracz, A. Opasinska, S. Kadlubowski, A. Krzywania-Kaliszewska, J. Grobelny, P. Wojciechowski, Dielectric Properties and Characterisation of Titanium Dioxide Obtained by Different Chemistry Methods, *Journal of Nanomaterials* 2014 (2014) 1–9.
- [74] D.C. Cronmeyer, M.A. Gilleo, The Optical Absorption and Photoconductivity of Rutile, *Phys. Rev.* 82 (1951) 975–976.
- [75] A. Levy, D. Andelman, H. Orland, Dielectric constant of ionic solutions: a field-theory approach, *Physical review letters* 108 (2012) 227801.
- [76] H. Shin, M.R. de Guire, A.H. Heuer, Electrical properties of TiO₂ thin films formed on self-assembled organic monolayers on silicon, *Journal of Applied Physics* 83 (1998) 3311–3317.
- [77] H. Kandel, J. Lu, J. Jiang, P. Chen, M. Matras, N. Craig, U.P. Trociewitz, E.E. Hellstrom, D.C. Larbalestier, Development of TiO₂ electrical insulation coating on Ag-alloy sheathed Bi₂Sr₂CaCu₂O_{8-x} round-wire, *Supercond. Sci. Technol.* 28 (2015) 35010.
- [78] K.-C. Kao, Dielectric phenomena in solids: With emphasis on physical concepts of electronic processes, Elsevier Academic Press, San Diego, 2004. ISBN: 0080470165 9780080470160
- [79] K.J. Laidler, J.H. Meiser, Physical chemistry, 2nd edition. Boston, Houghton Mifflin Company, 1995. ISBN: 0395641535 9780395641538
- [80] R. Morrow, D.R. McKenzie, M.M.M. Bilek, The time-dependent development of electric double-layers in saline solutions, *J. Phys. D: Appl. Phys.* 39 (2006) 937–943.
- [81] Scott Hughes, Lecture 7: Current, continuity equation, resistance, Ohm’s law: 7.4 Ohm’s law, MIT - Department of Physics, 24.02.05.

- [82] D. Zhang, Permeability enhancement by induced displacement current in magnetic material with high permittivity, *Journal of Magnetism and Magnetic Materials* 313 (2007) 47–51.
- [83] J. Golowasch, F. Nadim, Capacitance, Membrane, in: D. Jaeger, R. Jung (Eds.), *Encyclopedia of Computational Neuroscience*, Springer New York, New York, NY, 2013, pp. 1–5.
- [84] A. El-Gaddar, M. Frénéa-Robin, D. Voyer, H. Aka, N. Haddour, L. Krähenbühl, Assessment of 0.5 T static field exposure effect on yeast and HEK cells using electrorotation, *Biophysical journal* 104 (2013) 1805–1811.
- [85] M.A. Mansor, M.R. Ahmad, Single Cell Electrical Characterization Techniques, *International journal of molecular sciences* 16 (2015) 12686–12712.
- [86] G. Qiao, W. Duan, C. Chatwin, A. Sinclair, W. Wang, Electrical properties of breast cancer cells from impedance measurement of cell suspensions, *J. Phys.: Conf. Ser.* 224 (2010) 12081.
- [87] D. Wobschall, Voltage dependence of bilayer membrane capacitance, *Journal of Colloid and Interface Science* 40 (1972) 417–423.
- [88] O. Alvarez and R. Latorre, Voltage-dependent capacitance in lipid bilayers made from monolayers 21 (1978) 1–17.
- [89] K. Asami, Y. Takahashi, S. Takashima, Frequency domain analysis of membrane capacitance of cultured cells (HeLa and myeloma) using the micropipette technique, *Biophysical journal* 58 (1990) 143–148.
- [90] S.H. Wright, Generation of resting membrane potential, *Advances in physiology education* 28 (2004) 139–142.
- [91] K. Cheng, H.C. Haspel, M.L. Vallano, B. Osotimehin, M. Sonenberg, Measurement of membrane potentials (psi) of erythrocytes and white adipocytes by the accumulation of triphenylmethylphosphonium cation, *Journal of Membrane Biology* 56 (1980) 191–201.
- [92] A.M. Forsberg, J. Bergström, B. Lindholm, E. Hultman, Resting membrane potential of skeletal muscle calculated from plasma and muscle electrolyte and water contents, *Clinical science* (London, England 1979) 92 (1997) 391–396.
- [93] N. Mori, D. Wu, H. Furuta, Membrane potential in isolated epithelial cells of the endolymphatic sac in the guinea-pig, *Acta oto-laryngologica* 118 (1998) 192–197.
- [94] PhysiologyWeb, Goldman-Hodgkin-Katz Equation Calculator, www.physiologyweb.com. Accessed 27.07.2020
- [95] Y.W. Chow, R. Pietranico, A. Mukerji, Studies of oxygen binding energy to hemoglobin molecule, *Biochemical and biophysical research communications* 66 (1975) 1424–1431.
- [96] Lea Goetz and Christian Wilms, Understanding the cell as an electrical circuit: Combining R_m and C_m – the RC circuit, <https://www.scientifica.uk.com/learning-zone/understanding-the-cell-as-an-electrical-circuit>. Accessed 03.08.2020
- [97] A. Silve, I. Leray, C. Poignard, L.M. Mir, Impact of external medium conductivity on cell membrane electroporabilization by microsecond and nanosecond electric pulses, *Scientific reports* 6 (2016) 19957.

6. Curriculum Vitae

Mag. Terje Wimberger

Adress: Schweidlgasse 37/2/5, 1020 Vienna

Born 04.01.86 in Austria

Austrian and Norwegian citizen

Phone: 0043 676 47 288 26

Email: Terje.wimberger@ait.ac.at



Working experience

2018 – Date	AIT – Austrian Institute of Technology Junior Scientist – Advancing electroporation technology
2015 – 2018	AIT – Austrian Institute of Technology PhD Student – Innovative electric field treatments toward mammalian cell manipulation
2012 – 2013	CeMM – Center of Molecular Medicine of the National Academy of Science Diploma student in the field of molecular medicine
2010 – 2011	USG People Austria GmbH Technical customer support
2007 – 2010	Europ-Assistance GmbH Organization and monitoring of emergency operations for insured clients
2005 – 2007	Walter Mastermanagement GmbH Customer support for Tele2: Contract care and order processing

Education

2015 – 2020	BOKU - University of Natural Resources and Life Sciences PhD Candidate - Biotechnology
2014	ISO Certification as educational trainer for adults
2013	Diploma in molecular biology obtained with excellent success
2008 – Date	Qi-Tao martial arts: Wushu - Taiji Quan - Qi Gong 2015: Blackbelt and Co-trainer
2004 – 2013	University of Vienna Diploma program molecular biology
2004	School leaving examination with IB-Diploma (International Baccalaureate)

Publications

2020	Wimberger, Terje; Verena, Köhler K.; Ehmoser, Eva-Kathrin; Wassermann, Klemens J.. <i>Capacitive coupling increases the accuracy of cell-specific tumour ablation by electric fields</i> Bioelectrochemistry 2020 Feb 29;134:107495. doi: 10.1016/j.bioelechem.2020.107495
2019	Wimberger, Terje; Peham, Johannes R.; Ehmoser, Eva-Kathrin; Wassermann, Klemens J.. <i>Controllable cell manipulation in a microfluidic pipette-tip design using capacitive coupling of electric fields</i> . Lab Chip. 2019 Dec 7;19(23):3997-4006. doi: 10.1039/c9lc00927b.
2014	Riem Gawisch, Rui Martins, Benedikta Böhm, Terje Wimberger, Omar Sharif, Karin Lakovits, Mariane Schmidt, Sylvia Knapp. <i>Triggering receptor expressed on myeloid cell-2 fine-tunes inflammatory responses in murine Gram-negative sepsis</i> . FASEB J. 2015 Apr;29(4):1247-57. doi: 10.1096/fj.14-260067.
2010	Simon Stael, Agostinho G. Rocha, Terje Wimberger, Dorothea Anrather, Ute C. Vothknecht and Markus Teige. <i>Cross-talk between calcium signalling and protein phosphorylation at the thylakoid</i> . J Exp Bot. 2012 Feb;63(4):1725-33. doi:10.1093/jxb/err403

Patents filed

2020	Johannes Peham, Klemens Wassermann, Terje Wimberger; Coupled Sorting and Electric Treatment of Biological Cells; WO2020120650A1
2019	Johannes Peham, Klemens Wassermann, Terje Wimberger; Specific Electroporation and Lysis of Eukaryotic Cells; WO2020120651A1

Additional competence

Languages	German, native Norwegian, native English, proficient Swedish, conversational Danish, conversational
Software	MS Windows, MS Office (Word, Excel, PP, Outlook), Adobe Acrobat/Photoshop, SPSS, 3D Hyugens D&A Software, Zeiss ZEN Imaging, Graphpad Prism 7, Kaluza Flow Cytometry Analysis.

Vienna, November 2020